












REPORT



## Discovery of high affinity, pan-allelic, and pan-mammalian reactive antibodies against the myeloid checkpoint receptor SIRP $\alpha$

Janet Sim <sup>a</sup>, Jonathan T. Sockolosky <sup>a</sup>, Emma Sangalang <sup>a</sup>, Shelley Izquierdo<sup>b</sup>, Darlene Pedersen<sup>b</sup>, William Harriman<sup>b</sup>, Ardian S. Wibowo <sup>c</sup>, Josh Carter <sup>c</sup>, Anup Madan <sup>d</sup>, Laura Doyle <sup>a</sup>, Ons Harrabi<sup>a</sup>, Steven E. Kauder <sup>a</sup>, Amy Chen<sup>a</sup>, Tracy C. Kuo <sup>a</sup>, Hong Wan <sup>a</sup>, and Jaume Pons <sup>a</sup>

<sup>a</sup>ALX Oncology, Departments of Protein Sciences and Translational Biology, Burlingame, CA, USA; <sup>b</sup>Ligand Pharmaceuticals, Inc, Emeryville, CA, USA; <sup>c</sup>Helix Biostructures, Columbus, IN, USA; <sup>d</sup>Covance Genomics Laboratory, Redmond, WA, USA

### ABSTRACT

Targeting the CD47-signal-regulatory protein  $\alpha$  (SIRP $\alpha$ ) pathway represents a novel therapeutic approach to enhance anti-cancer immunity by promoting both innate and adaptive immune responses. Unlike CD47, which is expressed ubiquitously, SIRP $\alpha$  expression is mainly restricted to myeloid cells and neurons. Therefore, compared to CD47-targeted therapies, targeting SIRP $\alpha$  may result in differential safety and efficacy profiles, potentially enabling lower effective doses and improved pharmacokinetics and pharmacodynamics. The development of effective SIRP $\alpha$  antagonists is restricted by polymorphisms within the CD47-binding domain of SIRP $\alpha$ , necessitating pan-allele reactive anti-SIRP $\alpha$  antibodies for therapeutic intervention in diverse patient populations. We immunized wild-type and human antibody transgenic chickens with a multi-allele and multi-species SIRP $\alpha$  regimen in order to discover pan-allelic and pan-mammalian reactive anti-SIRP $\alpha$  antibodies suitable for clinical translation. A total of 200 antibodies were isolated and screened for SIRP $\alpha$  reactivity from which approximately 70 antibodies with diverse SIRP $\alpha$  binding profiles, sequence families, and epitopes were selected for further characterization. A subset of anti-SIRP $\alpha$  antibodies bound to both human SIRP $\alpha$  v1 and v2 alleles with high affinity ranging from low nanomolar to picomolar, potently antagonized the CD47/SIRP $\alpha$  interaction, and potentiated macrophage-mediated antibody-dependent cellular phagocytosis *in vitro*. X-ray crystal structures of five anti-SIRP $\alpha$  antigen-binding fragments, each with unique epitopes, in complex with SIRP $\alpha$  (PDB codes 6NMV, 6NMU, 6NMT, 6NMS, and 6NMR) are reported. Furthermore, some of the anti-SIRP $\alpha$  antibodies cross-react with cynomolgus SIRP $\alpha$  and various mouse SIRP $\alpha$  alleles (BALB/c, NOD, BL/6), which can facilitate preclinical to clinical development. These properties provide an attractive rationale to advance the development of these anti-SIRP $\alpha$  antibodies as a novel therapy for advanced malignancies.

**Abbreviations:** ADCC: antibody-dependent cellular cytotoxicity; ADCP: antibody-dependent cellular phagocytosis; CFSE: carboxyfluorescein succinimidyl ester; Fab: fragment antigen binding; Fc: fragment crystallizable; Fc $\gamma$ R: Fc $\gamma$  receptor; Ig: immunoglobulin; IND: investigational new drug; MDM $\phi$ : monocyte-derived macrophage; NOD: non-obese diabetic; scFv: single chain fragment variable; SCID: severe combined immunodeficiency; SIRP: signal-regulatory protein

### ARTICLE HISTORY

Received 1 February 2019  
Revised 16 April 2019  
Accepted 17 May 2019

### KEYWORDS


Antibody; SIRP $\alpha$ ;  
macrophage; phagocytosis;  
immunotherapy

### Introduction

Immune evasion is a hallmark of cancer, and therapeutic interventions that stimulate immune responses against tumors have shown remarkable clinical efficacy in diverse cancers.<sup>1,2</sup> In particular, antibodies targeting the T cell inhibitory receptors PD-1 and CTLA-4 are capable of inducing long term, durable antitumor immunity in humans by stimulating the adaptive arm of the immune system. However, many patients fail to respond or develop resistance to T cell checkpoint therapy because tumors exploit multiple mechanisms to avoid immune detection and destruction, including the suppression of innate immunity.<sup>3</sup> Combination therapies targeting non-redundant pathways that restrain antitumor immunity can dramatically improve response rates.

Signal-regulatory protein  $\alpha$  (SIRP $\alpha$ ) is an innate immune checkpoint receptor expressed primarily on myeloid cells, including monocytes, macrophages, dendritic cells (DCs), and neutrophils.<sup>4,5</sup> SIRP $\alpha$  suppresses innate immunity upon interaction with its ligand, CD47. CD47 is broadly expressed on normal tissues and is up-regulated by virtually all human tumors to escape macrophage recognition and programmed cell removal.<sup>6</sup> Inhibitory signals delivered by CD47 through SIRP $\alpha$  dampen Fc $\gamma$ R-dependent antibody effector functions, including macrophage and neutrophil-mediated antibody-dependent cellular phagocytosis (ADCP) and cytotoxicity (ADCC), limiting the induction of antibody-dependent innate immunity and promoting resistance to antitumor antibody therapy.<sup>6–9</sup>

**CONTACT** Jaume Pons  [jaume@alxoncology.com](mailto:jaume@alxoncology.com)  ALX Oncology, Burlingame, CA, USA

 Supplemental data for this article can be accessed on the [publisher's website](#).

© 2019 The Author(s). Published with license by Taylor & Francis Group, LLC.

This is an Open Access article distributed under the terms of the Creative Commons Attribution-NonCommercial-NoDerivatives License (<http://creativecommons.org/licenses/by-nc-nd/4.0/>), which permits non-commercial re-use, distribution, and reproduction in any medium, provided the original work is properly cited, and is not altered, transformed, or built upon in any way.

Antagonizing the CD47/SIRP $\alpha$  interaction has a profound impact on potentiation of macrophage and DC phagocytosis of antibody-opsonized tumor cells, which in turn can prime anti-tumor CD8 + T cell responses,<sup>10–12</sup> linking innate and adaptive immunity to anti-CD47 therapy. Beyond augmenting phagocytosis, disrupting the CD47/SIRP $\alpha$  interaction triggers numerous immunological responses that promote innate and adaptive antitumor immunity, including enhanced DC activation, a reduction in myeloid-driven immune suppression, and stimulation of type-I and type-II interferon responses.<sup>11–13</sup> When combined with either tumor antigen-specific or immunomodulatory antibodies targeting T cell inhibitory receptors, CD47/SIRP $\alpha$  antagonists dramatically improve response rates across numerous xenogeneic and syngeneic mouse cancer models, resulting in durable long-term tumor immunity.<sup>8,12,14–16</sup> Collectively, these preclinical results provide compelling evidence to support clinical evaluation of CD47/SIRP $\alpha$  antagonists in combination with antitumor or checkpoint antibodies. A variety of CD47 antagonists are under evaluation in the clinic.<sup>17</sup> Promising activity was recently reported for an anti-CD47 antibody used in combination with rituximab for the treatment of lymphoma.<sup>18</sup> In addition, the CD47 antagonist ALX148, a high-affinity SIRP $\alpha$  variant fused to an inactive Fc domain, has demonstrated a favorable safety profile and preliminary anti-cancer activity in the clinic when used in combination with pembrolizumab and trastuzumab for the treatment of solid tumors.<sup>12,19</sup>

Disrupting the CD47/SIRP $\alpha$  interaction initially focused on targeting CD47 due to its ubiquitous expression on human tumors;<sup>9,7</sup> however, several limitations associated with targeting CD47 may be circumvented by targeting SIRP $\alpha$ . The broad tissue distribution of CD47 creates a large antigen sink<sup>20</sup> and promotes target-mediated clearance of anti-CD47 antibodies. In contrast, SIRP $\alpha$  expression is predominately restricted to myeloid cells; therefore, targeting SIRP $\alpha$  enables reduced dosing to achieve maximal receptor occupancy and improved pharmacokinetic and pharmacodynamic (PK/PD) properties. Furthermore, anti-CD47 antibodies capable of triggering Fc effector functions cause dose-limiting toxicities, including anemia and thrombocytopenia due to CD47 expression on red blood cells and platelets.<sup>20,21</sup> Although we previously demonstrated that safety liabilities associated with anti-CD47 therapy can be avoided by Fc mutations that abrogate Fc $\gamma$ R and complement (C1q) binding,<sup>12,14</sup> it is of interest to study similarities and differences of an orthogonal approach to antagonize the SIRP $\alpha$ /CD47 axis by targeting SIRP $\alpha$ .<sup>4,9,16,22</sup>

SIRP $\alpha$  belongs to the SIRP family of immunoreceptors that include the highly homologous activating receptor SIRP $\beta$ 1 and the decoy receptor SIRP $\gamma$ .<sup>23</sup> Although CD47 is highly conserved, extensive polymorphisms localized to the CD47-binding IgV domain of SIRP $\alpha$  have been reported in numerous ethnic groups.<sup>24</sup> Initial investigation of SIRP $\alpha$  polymorphisms in humans identified 10 allelic variants of SIRP $\alpha$  with two prevalent alleles, v1 and v2, shared between diverse ethnic groups and eight additional alleles with population-specific distributions of unknown frequency.<sup>24</sup> More recently, Treffers et al. quantified SIRP $\alpha$  polymorphisms in Caucasians and identified only the two prevalent SIRP $\alpha$  variants, v1 and v2, within this population.<sup>25</sup>

Whereas genetic variation of SIRP $\alpha$  does not seem to affect intrinsic phagocyte function,<sup>25</sup> activation of a single functional SIRP $\alpha$  variant in heterozygote macrophages is sufficient to inhibit antibody-dependent effector functions.<sup>9</sup> Thus, effective therapeutic targeting of SIRP $\alpha$  across diverse patient populations requires pan-allelic anti-SIRP $\alpha$  antibodies.

We describe the discovery and characterization of a panel of wild-type, chimeric, and fully human anti-SIRP $\alpha$  monoclonal antibodies from chickens that exhibit high affinity, broad epitope coverage, and species cross-reactivity against mouse, monkey, and human SIRP $\alpha$  alleles. Guided by analysis of SIRP $\alpha$  polymorphisms across diverse human populations, we immunized chickens with allele and species-specific variants of SIRP $\alpha$  and screened antibody-secreting B cells to identify anti-SIRP $\alpha$  antibodies suitable for clinical translation. In total, 200 unique anti-SIRP $\alpha$  antibodies were identified and screened for binding to human, monkey, and mouse SIRP $\alpha$ , human SIRP $\beta$  and SIRP $\gamma$ , and for the ability to block the interaction between CD47 and SIRP $\alpha$ . Epitope binning and x-ray crystallography identified six distinct SIRP $\alpha$  epitopes, including epitopes that highly or partially overlap with the CD47 binding site, as well as epitopes that are distal from CD47. A subset of anti-SIRP $\alpha$  antibodies were found to bind with high affinity (nM to pM) to SIRP $\alpha$  v1 and v2 alleles, cross-react with monkey and mouse SIRP $\alpha$ , potentially antagonize the CD47/SIRP $\alpha$  interaction, and enhance macrophage phagocytosis of antibody-opsonized tumor cells. Thus, the anti-SIRP $\alpha$  antibodies described herein represent promising candidates for targeting the CD47/SIRP $\alpha$  immunoevasion pathway for the treatment of human cancers by unleashing innate and adaptive immune responses.

## Results

### **Two SIRP $\alpha$ allelic variants are prevalent in diverse human populations**

The distribution and frequency of SIRP $\alpha$  variants across population and ethnic groups are not well characterized. Successful therapeutic targeting of SIRP $\alpha$  in diverse patient populations irrespective of SIRP $\alpha$  genotype necessitates pan-allelic anti-SIRP $\alpha$  antibodies that cross-react with all relevant SIRP $\alpha$  alleles. To aid in the design of a pan-allelic anti-SIRP $\alpha$  antibody discovery strategy, we first sought to determine the distribution and frequency of SIRP $\alpha$  polymorphic variants in human populations. We initially turned to the 1000 Genome Project, which has the largest public repository of sequenced human genomes (<http://www.internationalgenome.org/home>), and performed a comprehensive bioinformatic analyses of the SIRP $\alpha$  gene from 2535 individuals from the Phase 3 dataset of the 1000 Genome Project.<sup>26</sup> As an orthogonal confirmation, we selected 510 individuals representing different populations from the above Phase 3 project, procured the respective DNA samples, and performed Sanger sequencing of exon 3 the SIRP $\alpha$  gene of these individuals. In agreement with Treffers et al.,<sup>25</sup> our bioinformatic analyses of SIRP $\alpha$  sequences from 2535 individuals and Sanger sequencing of 510 samples identified only two SIRP $\alpha$  variants, v1 and v2 (Table S1), represented as three allelic groups: homozygous v1/v1, homozygous v2/v2, and heterozygous v1/v2.

Examples of the detailed sequence analyses are described in Fig. S1. This contrasts with data reported by Takenaka et al.<sup>24</sup> who identified eight additional allelic variants besides v1 and v2. Since eight of these allelic variants and individuals analyzed by Takenaka et al.<sup>24</sup> were also coincidentally part of the Phase 3 dataset, we acquired the identical eight samples and carried out Sanger sequencing to confirm their allelic identities. Indeed, our results further confirmed that these samples are either homozygotes (v1/v1 or v2/v2) or heterozygotes (v1/v2).

Next, we determined the distribution and frequency of the SIRPα v1 and v2 allelic groups in various populations and their respective sub-populations (Figure 1(a,b)). The distribution of v1/v2 heterozygotes amongst the five super populations, European (EUR), American (AMR), East Asian (EAS), African (AFR) and South Asian (SAS), is similar and ranges from 42.0% to 47.2%. The East Asian population has a significantly higher number of v2/v2 than v1/v1 homozygotes occurring at a frequency of 42.3% and 13.3%, respectively, whereas the African, European, American, and South Asian populations had a moderately higher number of v1/v1 than v2/v2 homozygotes, with frequency ranges of 30.3–49.1% and 8.9–24.2%, respectively. The distribution of the three allelic variants within American, African, East Asian, South Asian and European sub-populations is similar to their respective super population, with the exception of the Peruvian (PEL) sub-population, which has a higher percentage of v2/v2 relative to v1/v1 homozygotes compared to the other American sub-populations (Figure 1(b)). Despite the observed distribution and frequency, we conclude only two SIRPα allelic variants v1 and v2 are present among the diverse populations analyzed in this study.

### Chicken immunization and GEM screen to isolate pan-allelic and -mammalian reactive anti-SIRPα antibodies

Based on our results from SIRPα polymorphism analyses, it is critical that anti-SIRPα antibodies are capable of binding both SIRPα v1 and v2 alleles to be useful for clinical development. In addition, to facilitate rapid preclinical to clinical translation, we sought to discover anti-SIRPα antibodies that also cross-react with mouse SIRPα alleles from strains commonly used for syngeneic and xenogeneic tumor models (e.g., NOD/SCID, BALB/c, C57BL/6), and cross-react with cynomolgus monkey SIRPα for

**Table 1.** Sequence identities of SIRPα IgV domains. The percentage amino acid sequence identities of IgV domains of SIRPα from human v1 (NP\_542970.1), human v2 (CAA71403.1), cynomolgus monkey (EHH65484.1), 129 mouse (162330193) and chicken (NP\_001032920.2) sources are listed, respectively. Percentage identity is calculated based on identical residues among all ungapped positions between sequence pairs. % Identity

	Human v1	Human v2	Cynomolgus Monkey	129 mouse	Chicken
Human v1		89	91	67	46
Human v2			88	69	41
Cynomolgus Monkey				74	47
129 mouse					47
Chicken					

toxicology studies that may enable an investigational new drug (IND) application. Based upon SIRPα sequence homology (Table 1, Fig. S2 and Fig. S3), it may be challenging to obtain human, cynomolgus monkey, and mouse cross-reactive antibodies through traditional mouse immunization methods. Chickens are an attractive alternative to mice because they are phylogenetically distant from humans,<sup>27,28</sup> and produce antibodies of high affinity and specificity that can recognize unique epitopes not accessible to mice.<sup>29</sup> Moreover, pan-mammalian-reactive anti-SIRPα antibodies are more likely to be discovered in chickens given the low homology between chicken SIRPα and the human and mouse orthologs (Table 1). The workflow for using chicken for immunization and antibody discovery is depicted in Figure 2(a).

To generate pan-allelic and species cross-reactive anti-SIRPα antibodies, we immunized wild-type and transgenic chickens with the extracellular IgV domain of human SIRPα allele v1, which is the sole extracellular domain that mediates interaction with CD47, followed by boosts that alternate between human SIRPα allele (v1 vs v2) and/or species (mouse NOD or 129 vs. human SIRPα) in order to drive antibody responses toward a cross-reactive repertoire (Table 2). Wild-type and two different transgenic chickens were used for immunization: SynVH chickens which contain humanized V<sub>H</sub> immunoglobulin (Ig) repertoires paired with the natural chicken light chain repertoire, and OmniChickens<sup>®</sup>, which contain humanized V<sub>H</sub> and V<sub>L</sub> Ig repertoires.<sup>30,31</sup> In total, eight immunized chickens produced high titer antibodies against SIRPα v1, v2 and mouse SIRPα (Table 2, Figure 2(b)) from which splenocytes were harvested, and single antibody-

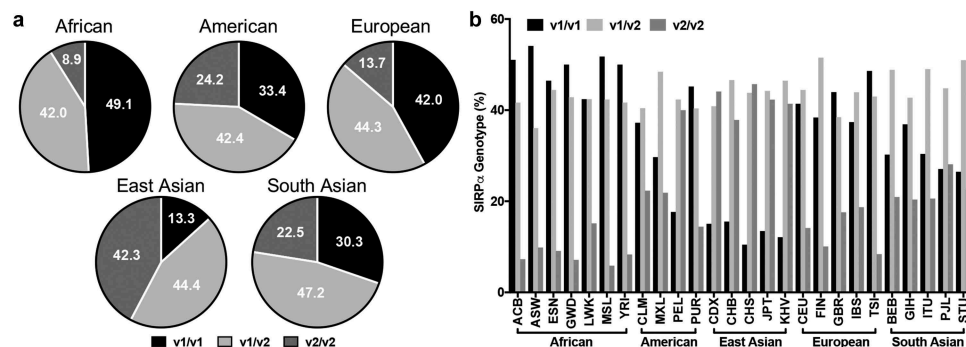


**Figure 1.** Frequency and distribution of SIRPα variants across human populations. The distribution and frequency of SIRPα alleles in the five super populations (a) and their respective subpopulations (b). In the 1000 Genome Project, the population from different locations around the globe are divided into five super populations as African (AFR), Ad Mixed American (AMR), East Asian (EAS), European (EUR) and South Asian (SAS). These super populations are further divided into total of 26 subpopulations. The code for the subpopulation can be found at <http://www.internationalgenome.org/category/population/>.

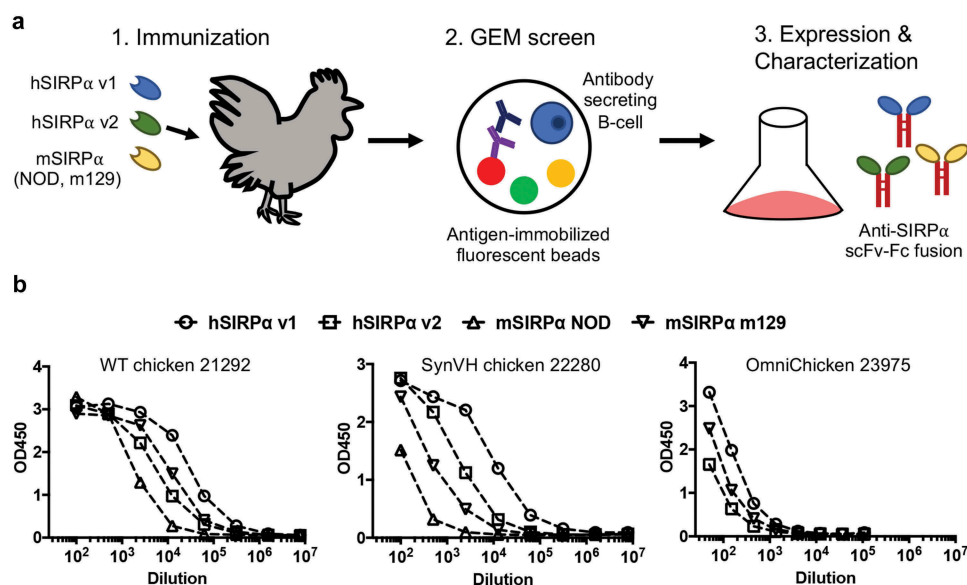


**Figure 2.** Isolation of anti-SIRP $\alpha$  antibodies from wild-type and transgenic chickens. (a) Schematic depicting the generation of pan-allele and pan-mammalian anti-SIRP $\alpha$  antibodies. (b) Plasma titers to hSIRP $\alpha$  v1, hSIRP $\alpha$  v2, mSIRP $\alpha$  NOD, and mSIRP $\alpha$  m129 in wild-type (left), SynVH (middle), and OmniChicken (right) chickens.

**Table 2.** Summary of the chicken immunization scheme and GEM screen results. Eight chickens (two wildtype, two SynVH and four OmniChickens) were immunized as described below. To drive response toward a cross-reactive repertoire, all the chickens were immunized by SIRP $\alpha$  allele v1 followed by boosts that alternate between human SIRP $\alpha$  allele (v1 vs v2) and/or species (mouse NOD or 129 vs. human SIRP $\alpha$ ). Various GEM screen combinations were used to facilitate the discovery of anti-SIRP $\alpha$  antibodies with unique binding profiles. A total of 200 chicken antibodies were cloned and the variable domain region sequenced.

Chicken	Immunization Scheme				GEM Screen			No. of scFv-Fc Isolated & Screened/Chicken <sup>a</sup>
	Initial 100ug	Boost 1 50ug	Boost 2 50ug	Boost 3 50ug	Bead 1	Bead 2	Bead 3	
WT 21288	V1	V2	V1	V2	V1	V2	NOD	34
WT 21292	V1	V2	m129	V1	V1	V2	Complex	9
					V2	m129	Complex <sup>c</sup>	
SynVH 22260	V1	V2	V1	V2	V1	V2	NOD	12
					V2	NOD	Complex	
SynVH 22280	V1	V2	m129	V1	V1	V2	M129	60
					V2	m129	Complex <sup>b</sup>	
					V2	BALBc	Complex	
					V2	Complex	Complex	
Omni 22843	V1	NOD	V2	NOD	V1	V2	SIRP $\gamma$	50
					V1	V2	Complex	
					V2	BALBc	Complex <sup>b</sup>	
					V2	Complex	Complex	
Omni 23504	V1	NOD	V2	NOD	V1	V2	Complex SIRP $\gamma$	4
Omni 23941	V1	NOD	V2	NOD	V1	V2	Complex	10
					V1	V2	SIRP $\gamma$	
Omni 23975	V1	NOD	V2	NOD	V1	V2	Complex SIRP $\gamma$	21
					V1	V2	Complex SIRP $\gamma$	

a. Total number of scFv-Fc screened by SPR from each chicken (from different GEM Screens).

b. Only two beads are used for these GEM screens.

c. Complex = CV1 and IgS domain of CD47 is pre-complexed before GEM screen.

secreting B-lineage cells were screened for reactivity toward SIRP $\alpha$  using a gel-encapsulated microenvironment (GEM) assay.<sup>32</sup>

The GEM assay consists of a single-antibody secreting B-cell encapsulated in a droplet containing up to three different fluorescent reporter beads, each coated with a target antigen of interest (Figure 2(a)). B-cell clones that produce antibodies that bind to the immobilized targets were detected with a secondary antibody against chicken IgY, visualized via fluorescent microscopy,

isolated, and sequenced. Various antigen-coated bead combinations were used to facilitate the discovery of anti-SIRP $\alpha$  antibodies with unique binding profiles (Table 2). For instance, to isolate pan-allelic and species-cross reactive antibodies that bind human SIRP $\alpha$  v1, human SIRP $\alpha$  v2, and mouse SIRP $\alpha$ , a triple-bead combination was used where each bead was individually coated with the respective antigen, and only B-cells producing antibodies that react with all three antigen-coated beads were recovered. Additional GEM screens were designed to distinguish

between antibodies that block the SIRP $\alpha$ /CD47 interaction and non-blocking antibodies via beads coated with SIRP $\alpha$  pre-complexed with CD47. Due to the weak affinity between wild-type SIRP $\alpha$  and CD47, we used engineered, high-affinity versions of SIRP $\alpha$  v1<sup>14</sup> and SIRP $\alpha$  v2 to ensure stability of the CD47/SIRP $\alpha$  complex and maximize the likelihood of identifying antibodies that bind SIRP $\alpha$  while in complex with CD47 (i.e., non-blocking antibodies). Conversely, blocking antibodies were identified by screening for clones that bind SIRP $\alpha$  but not the CD47/SIRP $\alpha$  complex, an indication that the antibody and CD47 bind overlapping epitopes on SIRP $\alpha$ . Through various GEM screens of lymphocytes prepared from immunized chickens (Table 2), over 200 unique anti-SIRP $\alpha$  antibody clones were identified. The V genes from each chicken antibody were reformatted into a single-chain variable fragment (scFv)-Fc fusion as described in Materials and Methods and produced recombinantly in HEK293FS for characterization by surface plasmon resonance (SPR) as described below.

### Chicken immunization yields anti-SIRP $\alpha$ antibodies with diverse binding properties, SIRP reactivity, and broad epitope coverage

We first characterized the binding kinetics and specificity of anti-SIRP $\alpha$  scFv-Fc fusions toward a panel of SIRPs including human SIRP $\alpha$  v1 and v2, cynomolgus monkey SIRP $\alpha$ , mouse SIRP $\alpha$  (m129, NOD, BL6 alleles), human SIRP $\gamma$ , and human SIRP $\beta$ 1. We performed a single concentration off-rate screen to triage anti-SIRP $\alpha$  scFv-Fc fusions based on species and allelic specificity, as well as cross-reactivity toward SIRP $\gamma$  and SIRP $\beta$ 1. Most anti-SIRP $\alpha$  scFv-Fc fusions were found to bind both human SIRP $\alpha$  v1 and v2 alleles and cross-react with cynomolgus monkey and mouse SIRP $\alpha$  (Table S2), in agreement with the designed immunization strategy and GEM screens. In addition to pan-allelic and species cross-reactive anti-SIRP $\alpha$  antibodies, we identified a subset of allele-specific and species-restricted anti-SIRP $\alpha$  antibodies with specificity for hSIRP $\alpha$  v1 (clones 1, 123, 179, and 194) or hSIRP $\alpha$  v2 (clone 110). In general, most anti-SIRP $\alpha$  antibodies also bound SIRP $\beta$ 1 and SIRP $\gamma$ , which was expected given the high degree of homology among SIRP family proteins (Fig. S4).

However, a small number of anti-SIRP $\alpha$  antibodies were identified that bind SIRP $\alpha$  and SIRP $\gamma$  but not SIRP $\beta$  (clones 1, 9, 93, 106), SIRP $\alpha$  and SIRP $\beta$ 1 but not SIRP $\gamma$  (clones 173, 174), and one specific for SIRP $\alpha$  with limited binding to SIRP $\beta$ 1 and SIRP $\gamma$  (clone 179). The specificity of anti-SIRP antibodies for SIRP $\alpha$ , SIRP $\beta$ , and SIRP $\gamma$  determined by SPR agrees with the reactivity of the anti-SIRP antibodies to various immune cell populations within human peripheral blood, which differ in expression of SIRP $\alpha$ , SIRP $\beta$ , and SIRP $\gamma$  (Fig. S7). Although outside the scope of this research, anti-SIRP $\alpha$  antibodies with differential specificity for SIRP $\alpha$ ,  $\beta$ , and  $\gamma$  may be useful tools to further explore the biology of the SIRP family of immunoreceptors.

Next, we determined the ability of anti-SIRP $\alpha$  scFv-Fc fusions to block the interaction between SIRP $\alpha$  and CD47. A competitive SPR-based binding assay was used whereby blocking and non-blocking antibodies were identified based upon their ability to bind SIRP $\alpha$  while in complex with CD47. Anti-SIRP $\alpha$  antibodies were first captured on a chip and increasing concentrations of CD47 (0 to 1500 nM) were added to a constant concentration of the high-affinity SIRP $\alpha$  v1 variant CV1<sup>14</sup> (100 nM) to pre-assemble the CD47:CV1 complex prior to injection over the antibody immobilized on a chip (Figure 3). At saturating concentrations of CD47 (>100 nM), antibodies that bind overlapping epitopes on SIRP $\alpha$  (blocking) fail to bind the SIRP $\alpha$ /CD47 complex, whereas antibodies that bind non-competitive epitopes (non-blocking) form a classical sandwich with the SIRP $\alpha$ /CD47 complex. A number of blocking and non-blocking antibodies were identified using this screen, as summarized in Table S2, and representative sensorgrams of a blocking and non-blocking antibody are depicted in Figure 3(a and b), respectively. In addition to blockers and non-blockers, a third category of anti-SIRP $\alpha$  antibodies was identified, termed kick-offs, that form a transient complex between antibody:SIRP $\alpha$ :CD47 prior to displacement of CD47 from antibody-bound SIRP $\alpha$  (Figure 3(c)). These antibodies bind SIRP $\alpha$  at a CD47 adjacent or minimally overlapping epitope<sup>33</sup> and trigger antigen exchange between antibody and CD47. This mechanism is supported by structural analysis presented below.

To determine the diversity of epitopes recognized by the isolated anti-SIRP $\alpha$  antibodies, we performed epitope binning using a classical sandwich-based SPR assay.<sup>34</sup> Binning experiments were conducted by immobilizing each anti-SIRP $\alpha$  antibody (ligand)

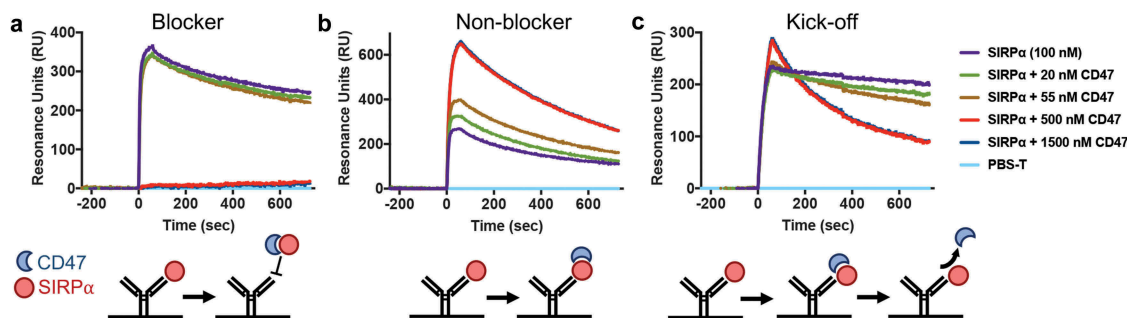


**Figure 3.** Surface plasmon resonance binding profiles of representative anti-SIRP $\alpha$  blocker, non-blocker, and kick-off antibodies. To assess if the anti-SIRP $\alpha$  antibodies can block CD47 binding to SIRP $\alpha$  *in vitro*, the antibodies were first captured by anti-human IgG-Fc on GLC chip as described in Materials and Methods. Next, 100 nM of a high-affinity SIRP $\alpha$  variant (CV1) pre-mixed with CD47 at concentrations of 0, 20, 55, 500, or 1500 nM were injected over the antibody-immobilized chip. The representative SPR sensorgrams for (a) blocking antibody clone 119, (b) non-blocking antibody clone 123, and (c) kick-off antibody clone 118 are shown. All sensorgrams were baseline-adjusted and reference cell-subtracted.

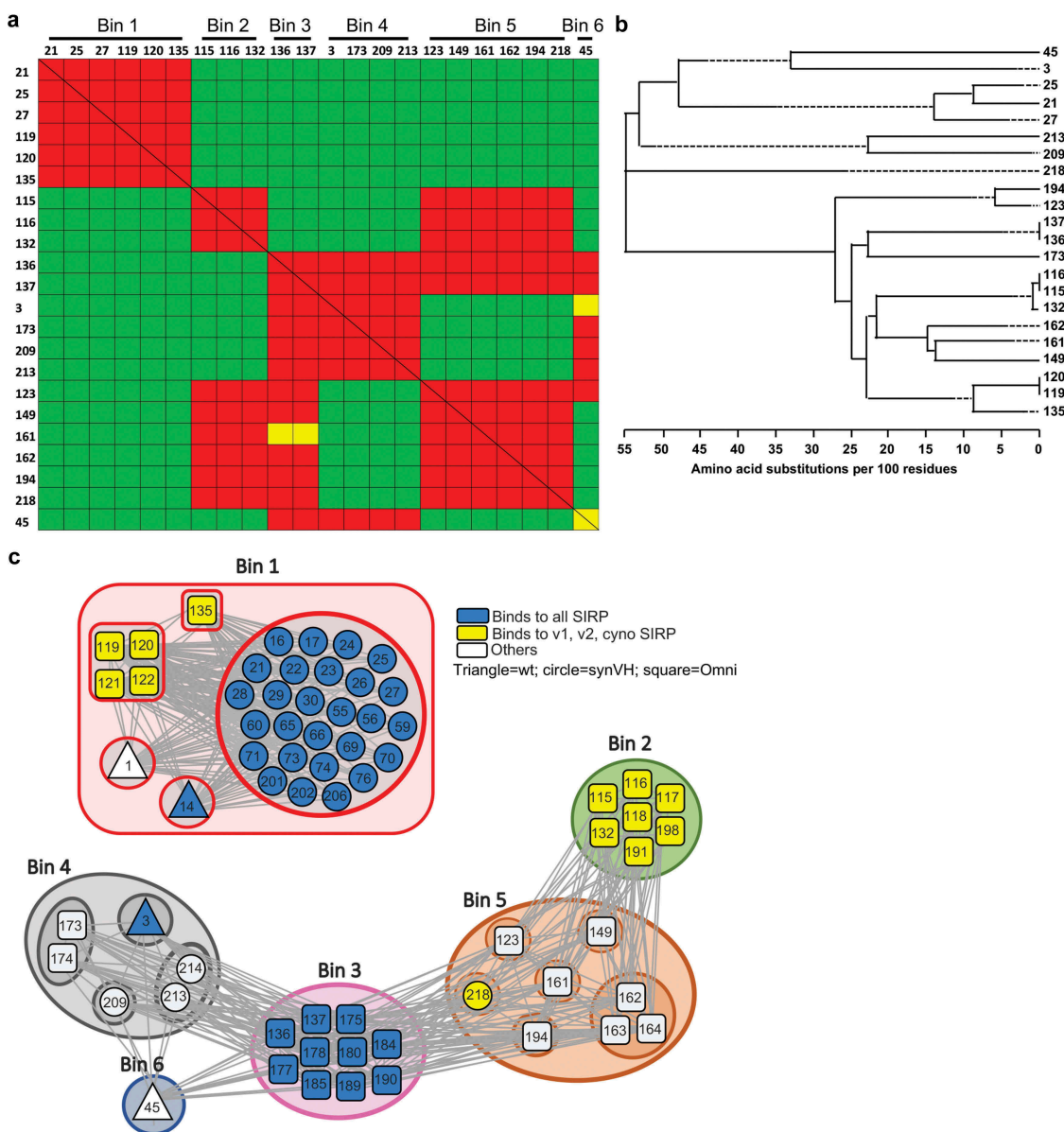


**Figure 4.** anti-SIRPa antibodies bind six unique epitopes on SIRPa. (a) Sorted heat map depicting the binning assignments for a representative subset of discovered anti-SIRPa antibodies. Anti-SIRPa antibodies bound to the chip are in rows and the anti-SIRPa antibodies injected over the chip in columns. Red boxes indicate that the antibodies compete with each other (and considered to bind the same epitope). Green boxes indicate that the antibodies form a sandwich (and considered to bind to different epitopes). Yellow boxes indicate scenarios where the data from one orientation disagrees with the other. (b) Phylogenetic tree for the subset of anti-SIRPa antibodies shown in (a). (c) Node plot illustrating the connectivity and blocking relationships between the anti-SIRPa antibodies in the six epitope bins. Antibodies isolated from wild-type, SynVH and OmniChickens are indicated as a triangle, circle, and square, respectively. Antibodies that bind to human, cynomolgus, and mouse SIRP (as well as SIRP $\beta$  and SIRP $\gamma$ ) are colored blue; those that bind to human SIRPa v1, v2, and cynomolgus SIRPa are colored yellow; and the remaining antibodies with varied specificities are colored white. Antibodies in Bin 1 do not cross-block antibodies in other bins. However, antibodies in bins 2, 3, 4, 5, 6 harbor cross-blocking properties indicated by the connecting grey lines.

followed by capture of the recombinant SIRPa antigen and the pairwise interrogation of an in-solution antibody (analyte) binding to the antibody-captured SIRPa antigen.<sup>34</sup> Epitope binning was performed again by reversing the mAb ligand/analyte orientation to validate the data set. A sorted heat map representing the epitope binning results for a panel of anti-SIRPa antibodies is shown in Figure 4(a). For simplicity, only representative antibodies within each bin are shown. Overall, the anti-SIRPa antibodies can be divided into six distinct epitope bins: blocking antibodies (bin 1), kick-off antibodies (bin 2), and non-blocking antibodies that subdivide into four bins (bin 3, 4, 5, and 6). The dendrogram showed that anti-SIRPa antibodies within the respective bins have

diverse VH/VL sequences (Figure 4(b)). To represent these cross-competition matrix relationships in a different dimension, a node plot was generated to emphasize the interconnectivities within and between each epitope bin, sequence diversity within each bin, SIRP reactivity, and the respective chicken from which the antibodies were isolated (Figure 4(c)). Interestingly, certain bins contain antibodies that segregate into diverse sequence groups and originate from different chickens, whereas other bins are sequence family and source specific. For instance, blocking antibodies (bin 1) were isolated from wild-type, SynVH, and OmniChickens with five distinct sequence lineages, whereas kick-off antibodies (bin 2) were only identified from OmniChickens and represent a single,

related sequence family (Figure 4(c)). Non-blocking antibodies segregated into four distinct bins (bins 3, 4, 5, and 6) with diverse sequence groups, SIRP reactivity, and interconnectivity between the various bins.

Epitope binning experiments also indicate anti-SIRP $\alpha$  antibodies in bin 1 do not cross-block anti-SIRP $\alpha$  antibodies in the other five bins, whereas anti-SIRP $\alpha$  antibodies in bins 2, 3, 4, 5, and 6 cross-block each other (Figure 4(a, c)). Therefore, anti-SIRP $\alpha$  antibodies in bin 1 are expected to bind non-overlapping epitopes compared to anti-SIRP $\alpha$  antibodies from the other bins. On the other hand, anti-SIRP $\alpha$  antibodies in bins 2, 3, 4, 5, and 6 are expected to share binding epitopes based on their cross-competition network. For instance, anti-SIRP $\alpha$  antibodies in bin 3 are expected to share certain binding site residues with anti-SIRP $\alpha$  antibodies in bin 5 but will share a different and unique set of overlapping binding residues with anti-SIRP $\alpha$  antibodies in bins 4 and 6, respectively. These observations were subsequently confirmed by structural analysis (Figure 5).

In summary, pan-allele and -mammalian reactive anti-SIRP $\alpha$  blocking and non-blocking antibodies (blue nodes) could be identified from both wild-type and transgenic chickens; the use of multiple chickens with different Ig repertoires enabled the discovery of a collection of anti-SIRP $\alpha$  antibodies with broad epitope coverage and sequence diversity.

### **Crystal structures of anti-SIRP $\alpha$ Fab fragments in complex with SIRP $\alpha$**

To further confirm results from epitope binning and map the binding site details, as well as to elucidate the structural mechanisms underlying the effects of anti-SIRP $\alpha$  antibodies, we determined the crystal structures of representative anti-SIRP $\alpha$  Fabs from epitope bins 1–5 in complex with the IgV domain of human SIRP $\alpha$  v1. The antibodies include the blocking antibody 119 (bin 1), kick-off antibody 115 (bin 2), and non-blocking antibodies 136 (bin 3), 3 (bin 4), and 218 (bin 5). High-resolution crystals (1.83–2.68 Å) were obtained for all fiveFab:SIRP $\alpha$  complexes, and the corresponding structures were solved by molecular replacement<sup>35</sup> (Figure 5(a), Table S4).

The anti-SIRP $\alpha$  blocking antibody clone 119 (bin 1) binds on top of SIRP $\alpha$  at an epitope highly overlapping that of CD47, in agreement with the antagonistic properties of clone 119 (Figure 5(b)). Although the binding geometries of CD47 and clone 119 to SIRP $\alpha$  are different, both proteins interact with a number of shared residues on SIRP $\alpha$  distributed throughout the binding interfaces (Figure 5(b, c)). Clone 119 binds SIRP $\alpha$  in a “top-down” orientation inserting its CDR-H3 loop into a central pocket of SIRP $\alpha$  formed by the BC, C'D, and DE loops (Figure 5(b)), occupying the same site as the CD47 N-terminal pyroglutamate (pE), which contributes significantly to interaction between CD47 and SIRP $\alpha$ , whereas CD47 binds SIRP $\alpha$  in a “lying-down” orientation inserting its FG loop into a wide groove on the surface of SIRP $\alpha$ .<sup>35</sup>

The non-blocking antibodies 3, 136, and 218 bind SIRP $\alpha$  at regions distal from the CD47 binding site and do not overlap with any residues on SIRP $\alpha$  involved in either CD47 or clone 119

binding (Figure 5(a, c)), consistent with results obtained from epitope binning (Figure 4(a, c)). Anti-SIRP $\alpha$  clones 3, 136, and 218 interact with three unique but interconnected epitopes on SIRP $\alpha$  (Figure 5(c)). Clone 136 occupies a central SIRP $\alpha$  epitope flanked on opposing sides by clones 3 and 218, which bind distinct epitopes on SIRP $\alpha$  that partially overlap with clone 136, but not with each other. These crystallographic findings are consistent with the cross-competition network between clone 136 (bin 3), clone 3 (bin 4), and clone 218 (bin 5). Clone 136 competes with both clone 3 and 218 for SIRP $\alpha$  binding, whereas clones 3 and 218 compete with clone 136, but not with each other (Figure 4(a, c)).

Interestingly, the “kick-off” antibody clone 115 binds SIRP $\alpha$  directly underneath CD47 at a site mostly independent from that of CD47, with the exception of one residue localized to the C'D loop of SIRP $\alpha$ , Glu54, which is shared by both 115 and CD47 (Figure 5(c, d)). Superposition of the CD47:SIRP $\alpha$  and 115:SIRP $\alpha$  interfaces reveals remodeling of the C'D loop to an orientation that is favorable for binding to its respective ligand, as well as potential steric clashes between clone 115 and CD47 that could prevent CD47 from remaining bound to SIRP $\alpha$  upon antibody association (Figure 5(d)). It is conceivable that clone 115 first engages SIRP $\alpha$  while bound to CD47, potentially initiated by interactions between clone 115 and SIRP $\alpha$  that are distal from CD47, which ultimately leads to displacement of CD47 due to steric clashes between the heavy chain framework 3 regions (HC-FR3) of clone 115 and CC' loop of CD47 (Figure 5(d)). This agrees with results from the SPR screen, where a transient increase in resonance was observed, indicating formation of the ternary complex between clone 115:CD47:SIRP $\alpha$ , and subsequent decrease in resonance consistent with the displacement of CD47 from the antibody/SIRP $\alpha$  complex (Figure 3(c)). Similar allosteric and displacement effects of an anti-IL-2 antibody that modulates cytokine–receptor interactions have been described<sup>36</sup> as well as for anti-EGFR antibodies that target closely adjacent epitopes.<sup>33</sup> In addition to overlapping epitopes with CD47, clone 115 partially overlaps with clone 218 (Figure 5(a) and Fig. S5), consistent with results obtained from epitope binning (Figure 4(a, c)).

We solved the structures of anti-SIRP antibodies in complex with the hSIRP $\alpha$  v1 allele; however, the structures of SIRP $\alpha$  v1 and v2 are highly conserved,<sup>35</sup> and only 1 or 2 of the 13 polymorphic residues contribute interactions with the anti-SIRP $\alpha$  antibodies (Table S3). Therefore, we suspect the antibodies will bind hSIRP $\alpha$  v2 in a similar orientation, although this needs to be validated through future crystallographic analyses.

### **Anti-SIRP $\alpha$ antibodies bind with high affinity to SIRP $\alpha$**

Based on epitope binning and mapping, SIRP reactivity, and sequence diversity, we selected a subset of antibody clones for expression as full-length IgG molecules for further characterization. Binding affinities ( $K_D$ , M) as determined by SPR of representative anti-SIRP $\alpha$  antibodies from each epitope bin are summarized in Table 3. All antibodies bound to human SIRP $\alpha$  v1 and v2 with high affinity ranging from low nanomolar to picomolar. To facilitate clinical development, we prioritized

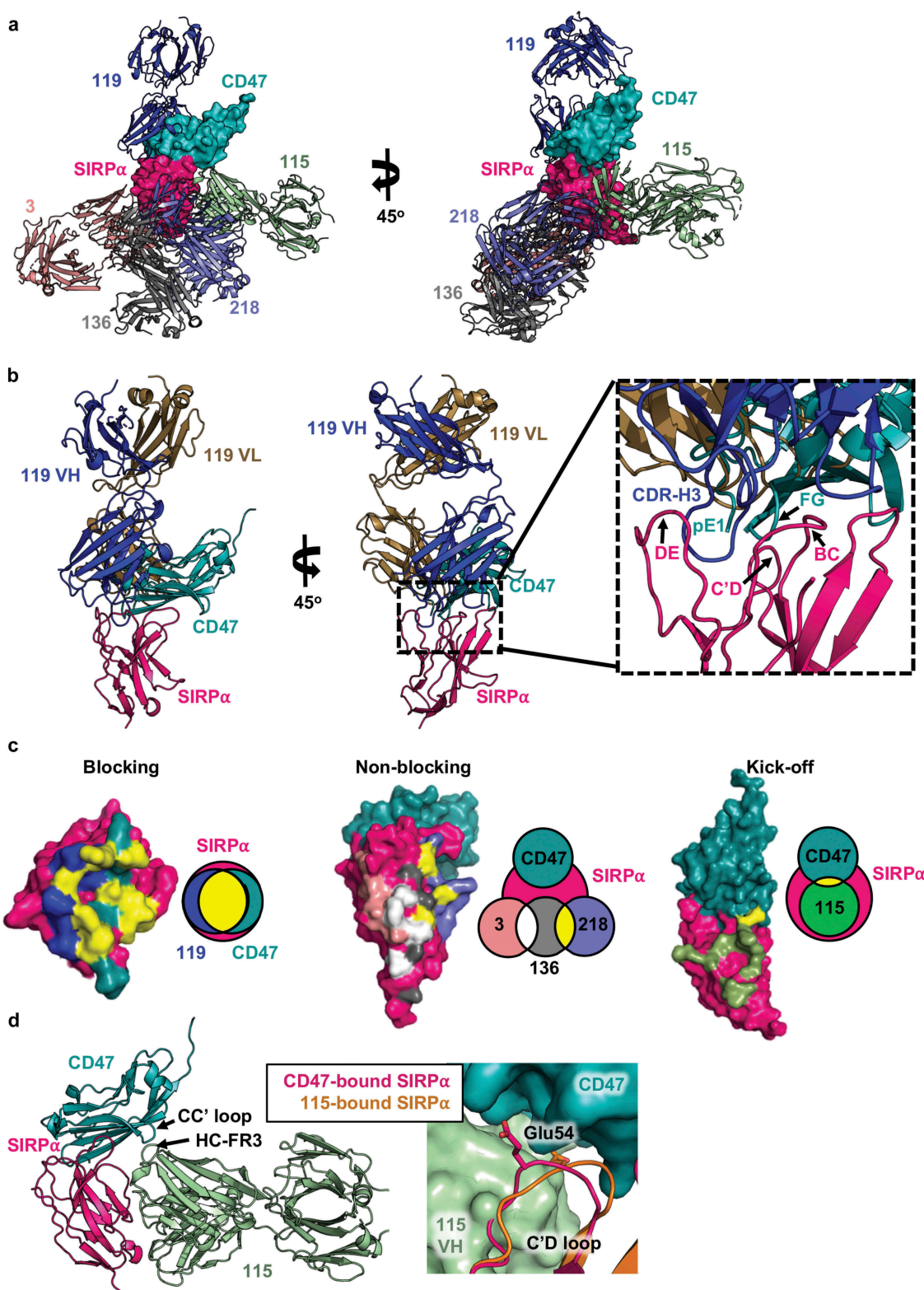


**Figure 5.** Crystal structures of anti-SIRP $\alpha$  antibodies bound to the IgV-domain of hSIRP $\alpha$  v1. (a) Structure of the SIRP $\alpha$  (pink)-CD47 (teal) complex superimposed with the anti-SIRP $\alpha$  blocking antibody Fab clone 119 (blue), non-blocking antibody Fabs clones 3 (pale pink), 136 (grey), and 218 (purple), and kick-off antibody Fab 115 (light green). (b) Overlay of the CD47/SIRP $\alpha$  complex and the blocking antibody clone 119 complex with a detailed view of CDR-H3 insertion into SIRP $\alpha$  pocket shown on the right. (c) Depiction of SIRP $\alpha$  (pink) epitopes bound by CD47 (teal) and anti-SIRP $\alpha$  antibody clones 119 (blue), 3 (pale pink), 136 (grey), 218 (purple), and 115 (light green). Residues shared between the blocking (119) and kick-off (115) antibodies and CD47 are colored yellow. Venn diagrams adjacent to each surface map indicate the relative extent of overlap between the blocking Fab 119 anti-SIRP $\alpha$  antibody, SIRP $\alpha$ , and CD47. For non-blocking antibodies, the yellow and white in the Venn diagrams indicate the overlap of epitopes between Fab 3, 136, and 218. (d) Overlay of the kick-off antibody clone Fab 115 (light green) and CD47 (teal) in complex with SIRP $\alpha$  (pink). The inset to the right shows the position of the C'D loop of SIRP $\alpha$  in the CD47-bound (pink) complex or the Fab 115-bound (orange) complex. The Glu 54 residues is modeled in the C'D loop to highlight the varying position depending on whether the binding partner is CD47 or Fab 115.



**Table 3.** Binding affinities  $K_D$  (M) of representative anti-SIRP $\alpha$  antibodies. Representative clones from each epitope bin were selected and their binding affinities to various SIRP (human SIRP $\alpha$  v1, v2; cynomolgus SIRP $\alpha$ ; mouse NOD, BL6, BALB/c SIRP $\alpha$ ; human SIRP $\gamma$ ; human SIRP $\beta$ 1) were determined by SPR. A Langmuir kinetic model was used for fitting and calculation of  $K_D$  (M). The ability of the antibody to block CD47 binding to SIRP $\alpha$  is indicated in the last column.

Bin	Antibody <sup>1</sup>	Source <sup>4</sup>	V1	V2	Cyno	NOD	BL6	BALB/c	SIRP $\gamma$	SIRP $\beta$ 1	CD47 Blocking
1	119	H	1.83E-10	6.82E-11	1.12E-10	NB <sup>2</sup>	NB	NB	2.67E-10	3.42E-10	Block
1	135	H	1.51E-10	2.90E-11	9.69E-11	NB	NB	NB	5.39E-10	1.10E-10	Block
1	21	S	<1.00E-12	<1.00E-12	3.61E-12	5.47E-10	4.60E-10	1.05E-09	<1.00E-12	<1.00E-12	Block
2	115	H	4.26E-10	1.86E-09	2.41E-09	NB	NB	NB	B <sup>3</sup>	B	Kick-off
3	136	H	4.58E-10	1.63E-09	2.15E-09	5.54E-10	1.27E-08	3.50E-10	2.39E-08	4.35E-09	Non-block
4	3	W	1.62E-10	7.67E-11	2.29E-09	1.63E-09	3.65E-09	1.16E-09	8.36E-08	1.63E-09	Non-Block
4	173	H	9.37E-10	9.28E-09	4.46E-08	NB	NB	NB	NB	B	Non-Block
4	209	S	1.71E-10	5.01E-09	3.90E-08	NB	NB	NB	8.99E-09	B	Non-Block
4	213	S	6.05E-09	1.69E-09	4.49E-08	NB	NB	NB	2.02E-09	1.71E-08	Non-Block
5	123	H	6.05E-10	NB	1.62E-09	NB	NB	NB	7.47E-10	7.07E-08	Non-Block
5	149	H	8.73E-10	2.38E-10	7.64E-09	NB	NB	NB	1.89E-09	2.06E-10	Non-Block
5	161	H	1.03E-09	1.27E-10	6.35E-09	NB	NB	NB	2.84E-09	2.63E-09	Non-Block
5	162	H	4.50E-10	1.57E-08	1.26E-08	NB	NB	NB	3.97E-09	3.00E-09	Non-Block
5	194	H	4.97E-10	NB	9.11E-10	NB	NB	NB	9.47E-10	5.36E-08	Non-Block
5	218	S	1.23E-10	2.76E-10	5.99E-11	NB	NB	NB	6.36E-11	B	Non-Block
6	45	W	6.63E-11	1.34E-10	NB	NB	NB	NB	2.71E-08	1.06E-08	Non-Block

1. All antibodies are screened as full IgG1 except 173, 209, 213, 123, 149, 161, 162, 194, 218 are screened as scFv-Fc.

2. NB = no binding

3. B = binding confirmed and exact  $K_D$  value was not determined.

4. W = wt, H = OmniChicken, S = SynVH chickens.

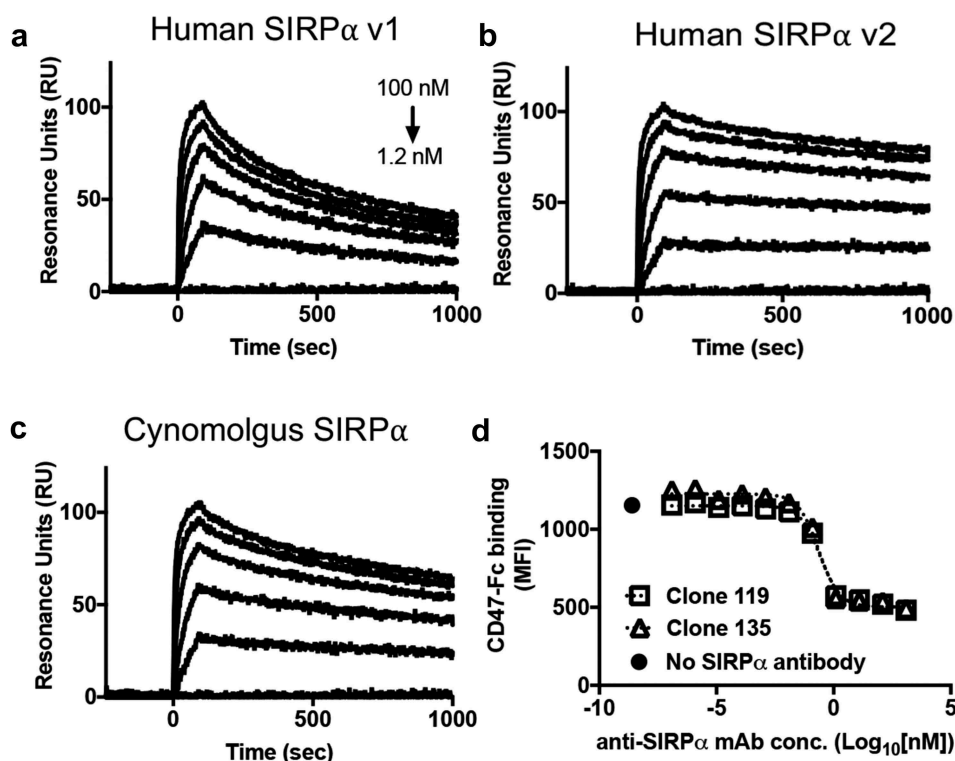


**Figure 6.** Anti-SIRP $\alpha$  blocking antibody clone 119 binds with high affinity to human and cynomolgus SIRP $\alpha$  and potentially blocks CD47 binding to cell surface SIRP $\alpha$ . (A-C) SPR analysis of the binding kinetics of anti-SIRP $\alpha$  antibody clone 119 binding to (a) hSIRP $\alpha$  v1, (b) hSIRP $\alpha$  v2, and (c) cynomolgus SIRP $\alpha$ . (d) Competition assay depicting dose-dependent antagonism of CD47-Fc binding to human CD14<sup>+</sup> monocytes by anti-SIRP $\alpha$  blocking antibody clones 119 and 135.

anti-SIRP $\alpha$  antibodies that bind similarly to both human SIRP $\alpha$  alleles and to cynomolgus SIRP $\alpha$ . The blocking antibody clones 21, 119, and 135 bind human SIRP $\alpha$  v1 and v2 alleles and cynomolgus SIRP $\alpha$  with a  $K_D$  of  $\sim$ 1 pM and 100 pM, respectively (Figure 6(a, b)). Clones 119 and 135 potentially antagonize the SIRP $\alpha$ /CD47 interaction with an  $IC_{50}$  of  $\sim$ 0.3 nM (Figure 6(d)). Whereas clones 119 and 135 are specific for human and cynomolgus monkey SIRP $\alpha$ , clone 21 cross-reacts with mouse SIRP $\alpha$  alleles, albeit with somewhat reduced affinity ( $K_D \sim$  0.5–1 nM) (Table 3). In addition, the non-blocking anti-SIRP $\alpha$  antibody

clone 136 binds human SIRP $\alpha$  v1 and v2 alleles and cynomolgus SIRP $\alpha$  similarly with a  $K_D$  of  $\sim$ 1 nM. Clone 136 also cross-reacts with mouse SIRP $\alpha$  alleles with affinities comparable to that of human SIRP $\alpha$  ( $\sim$ 1 nM). Of the antibodies that bind human and cynomolgus SIRP $\alpha$ , three also bind with high affinity to mouse SIRP $\alpha$  alleles from NOD, C57BL/6, and BALB/c: one blocking antibody (clone 21) and two non-blocking antibodies (clones 3 and 136) (Table 3). High-affinity binding of anti-SIRP $\alpha$  antibodies to all three mouse SIRP $\alpha$  alleles are particularly attractive as this enables the interrogation of SIRP $\alpha$  antagonism across

diverse preclinical mouse xenogeneic and syngeneic cancer models in the NOD/SCID, C57BL/6, BALB/c backgrounds. In summary, a large panel of antibodies with diverse binding specificities toward human, cynomolgus, and mouse SIRP $\alpha$ , as well as SIRP isoforms (SIRP $\beta$ 1, SIRP $\gamma$ ), broad epitope coverage, and antagonistic properties were successfully identified in this study.

### Anti-SIRP $\alpha$ antibodies potentiate macrophage phagocytosis of human tumor cells

Next, we evaluated the ability of anti-SIRP $\alpha$  antibodies to potentiate macrophage-mediated ADCP in combination with tumor-specific antibodies. We mutated anti-SIRP $\alpha$  antibody Fc-domains to abrogate binding to all Fc $\gamma$ Rs and complement<sup>37,38</sup> in order to decouple potential Fc $\gamma$ R- and complement-dependent contributions of anti-SIRP $\alpha$  antibodies to ADCP from direct inhibition of SIRP $\alpha$  signaling. Human monocyte-derived macrophages were incubated with carboxyfluorescein succinimidyl ester (CFSE)-labeled DLD-1 tumor cells opsonized with the tumor antigen-specific (anti-epidermal growth factor receptor (EGFR)) antibody cetuximab alone or in combination with increasing concentrations of anti-SIRP $\alpha$  blocking (clone 119) or non-blocking (clone 136) antibodies and phagocytosis was quantified by flow cytometry. Untreated DLD-1 cells were poorly phagocytosed, but treatment with cetuximab induced a significant increase in macrophage phagocytosis, which was

further enhanced in a dose-dependent manner by the SIRP $\alpha$  antagonist (blocking) antibody clone 119 (Figure 7(a)). Somewhat surprisingly, the non-blocking anti-SIRP $\alpha$  antibody clone 136 also potentiated phagocytosis in combination with cetuximab (Figure 7(a)). Enhancement of phagocytosis by non-blocking anti-SIRP $\alpha$  antibodies was not specific to clone 136. All anti-SIRP $\alpha$  non-blocking antibodies, irrespective of epitope, potentiated cetuximab-mediated phagocytosis, albeit with varying degrees of potency (Figure 7(b)). Potentiation of phagocytosis by both blocking and non-blocking anti-SIRP $\alpha$  antibodies was not dependent on the presence of an Fc domain, as F(ab')<sub>2</sub> fragments of clone 21 (blocking) and clone 136 (non-blocking) similarly enhanced phagocytosis compared to their full-length IgG counterparts (Figure 7(c)). Treatment with either intact anti-SIRP $\alpha$  antibodies or F(ab')<sub>2</sub> fragments of the non-blocking antibodies had little to no impact on macrophage cell surface SIRP $\alpha$  levels (Fig. S6), indicating that phagocytosis by non-blocking antibodies was not due to SIRP $\alpha$  downregulation. Anti-SIRP $\alpha$  blocking and non-blocking antibodies similarly enhanced macrophage phagocytosis of OE19 cells opsonized with the antitumor (anti-human epidermal growth factor receptor 2) antibody trastuzumab (Figure 7(b)).

SIRP $\beta$  is an activating receptor with a high degree of homology to SIRP $\alpha$  (Fig. S4), therefore many of the discovered antibodies cross-react with SIRP $\beta$ . Antibodies against SIRP $\beta$  have been reported to enhance mouse macrophage

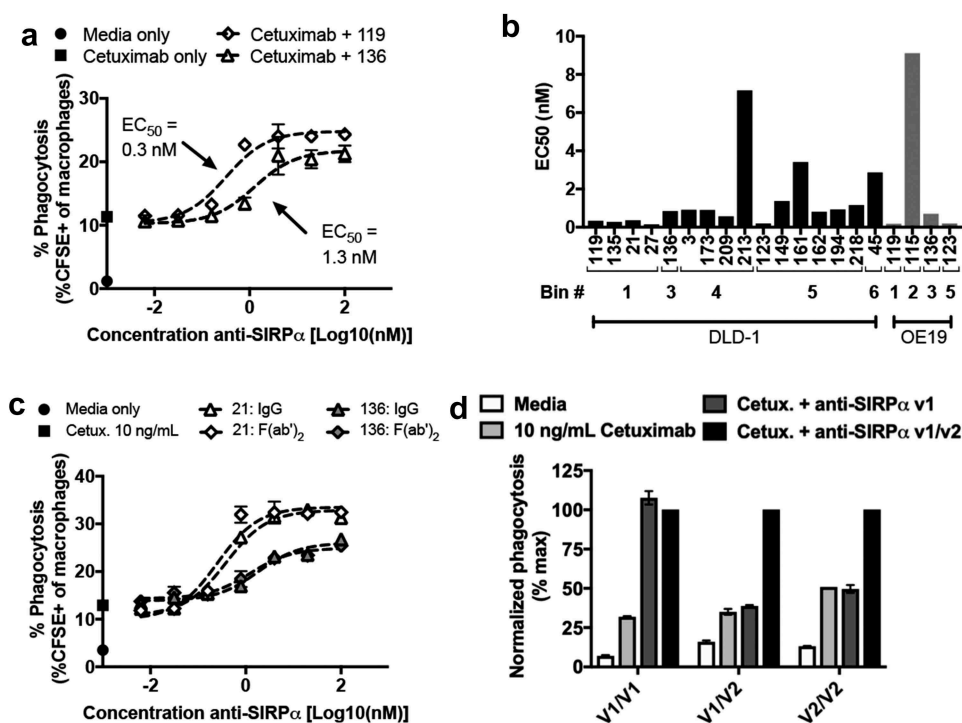


**Figure 7.** Anti-SIRP $\alpha$  antibodies potentiate macrophage-mediated ADCP in vitro. (a) Phagocytosis of DLD-1 cells by human monocyte-derived macrophages treated with the tumor-specific, anti-EGFR antibody cetuximab alone (closed square) or in combination with anti-SIRP $\alpha$  blocking (clone 119) or non-blocking (clone 136) antibodies. (b) Bar graph depicting the EC<sub>50</sub> of phagocytosis (as shown in a) of anti-SIRP $\alpha$  antibodies from various epitope bins. Bin 1 = blocking, bin 2 = kick-off, and bins 3–6 = non-blocking. Phagocytosis was conducted using DLD-1 cells as targets with cetuximab in combination with anti-SIRP $\alpha$  antibodies (black bars), or OE19 target cells with trastuzumab in combination with anti-SIRP $\alpha$  antibodies (grey bars). (c) Dose-dependent enhancement of DLD-1 phagocytosis by human monocyte-derived macrophages treated with cetuximab in combination with anti-SIRP $\alpha$  intact IgG antibodies (blocking clone 21 and non-blocking clone 136) or the corresponding F(ab')<sub>2</sub> fragments. (d) Macrophage phagocytosis of DLD-1 cells treated with cetuximab alone or in combination with the hSIRP $\alpha$  v1 allele-specific antibody<sup>39</sup> or pan-allele reactive anti-SIRP $\alpha$  v1/v2 antibody clone 21 as a function of macrophage SIRP $\alpha$  genotype. Data are normalized to the maximum phagocytosis observed in the clone 21 group. Data in panels A, C, and D are the mean (n = 3), and error bars indicate SD. Dashed lines represent data fit to a log-agonist vs. response model in Prism.

phagocytosis of IgG-opsonized sheep red blood cells *in vitro*, although phagocytosis was enhanced only in the presence of secondary cross-linking antibodies, suggesting higher order SIRP $\beta$  clustering is necessary to promote phagocytosis.<sup>40</sup> Nonetheless, to investigate the contribution of SIRP $\beta$  to anti-SIRP antibody-mediated macrophage phagocytosis, we profiled the human macrophages used in our assay for expression of SIRP $\alpha$ , SIRP $\beta$ , and SIRP $\gamma$ , and conducted phagocytosis assays using anti-SIRP $\alpha$  antibodies that do not bind to SIRP $\beta$ : clone 179 (SIRP $\alpha$  specific), and clone 1 (SIRP $\alpha$  and SIRP $\gamma$  specific). SIRP $\beta$  was expressed on human CD14<sup>+</sup> monocytes but was not expressed on the monocyte-derived macrophages (MDM $\phi$ ) used in our assay (Fig. S8A). SIRP $\gamma$  was expressed on CD3<sup>+</sup> T cells, but not CD14<sup>+</sup> monocytes or MDM $\phi$ . The anti-SIRP $\alpha$  antibody clones 1 and 179, which do not bind SIRP $\beta$ , potentiated cetuximab-mediated macrophage phagocytosis of DLD-1 cells in a dose-dependent manner similar to the activity of the pan-SIRP antibody clone 21 (Fig. S8B). Collectively, our data indicate that the phagocytic activity of the anti-SIRP antibodies used in this study is mediated by SIRP $\alpha$  and not due to cross-reactivity with SIRP $\beta$ .

Furthermore, SIRP $\alpha$  allele cross-reactivity was crucial to the efficacy of anti-SIRP $\alpha$  antibodies (Figure 7(d)). The anti-SIRP $\alpha$  v1 allele-specific antibody potentiated tumor cell phagocytosis by v1/v1 homozygous macrophages but failed to enhance phagocytosis mediated by v1/v2 heterozygous or v2/v2 homozygous macrophages. In contrast, the pan-allele anti-SIRP $\alpha$  v1/v2 antibody potentiated ADCP independent of macrophage SIRP $\alpha$  genotype (Figure 7(d)). These data are consistent with that of Zhao et al. who demonstrated that a single functional allele of SIRP $\alpha$  was sufficient to inhibit neutrophil-mediated killing of antibody-opsonized tumor cells.<sup>9</sup> Thus, therapeutic targeting of SIRP $\alpha$  requires pan-allelic antibodies in order to be useful in diverse patient populations.

## Discussion

The CD47-SIRP $\alpha$  axis has emerged as a myeloid checkpoint pathway to be targeted for the treatment of human cancers, and an ensuing plethora of agents aimed at disrupting the CD47-SIRP $\alpha$  interaction have entered the clinic or are in preclinical development.<sup>17</sup> We previously demonstrated that ALX148, a high-affinity variant of hSIRP $\alpha$  fused to an inactive Fc-domain of IgG, potently antagonizes CD47, is well tolerated in preclinical species and has a favorable safety profile in humans due to the lack of Fc-effector function,<sup>12,19</sup> is efficacious in numerous xenogeneic and syngeneic mouse cancer models when used in combination with tumor-specific and checkpoint antibodies,<sup>12</sup> and has promising preliminary anti-tumor activity in humans.<sup>19</sup> ALX148 prevents SIRP $\alpha$  signaling by occupying CD47, both on the tumor and in the periphery. CD47 is broadly expressed and has numerous reported ligands and functions beyond SIRP $\alpha$ -dependent regulation of macrophages and dendritic cells.<sup>23</sup> The functional differences between targeting SIRP $\alpha$  and CD47 are generally unknown in part due to a lack of specific reagents that antagonize SIRP $\alpha$ . Thus, we sought to generate and characterize anti-SIRP $\alpha$  antibodies with diverse properties in order to investigate

SIRP $\alpha$  biology and extend our approach of antagonizing the CD47/SIRP $\alpha$  interaction as a treatment modality for cancer to SIRP $\alpha$ .

The development of effective SIRP $\alpha$  antagonists suitable for clinical translation has been challenging due to the polymorphic nature of SIRP $\alpha$  as well as a poor understanding of the allelic distribution and frequency of SIRP $\alpha$  across human populations. Zhao et al. previously demonstrated using pan-allelic or allele-specific anti-SIRP $\alpha$  blocking antibodies that antagonism of both SIRP $\alpha$  alleles was necessary to enhance trastuzumab-mediated ADCC when neutrophils from SIRP $\alpha$  v1/v2-heterozygous donors were used as effector cells.<sup>9</sup> We observed a similar requirement for antagonism of both SIRP $\alpha$  alleles to enhance macrophage-mediated ADCP when v1/v2-heterozygous macrophages were used as effectors (Figure 7(d)), in agreement with results by Zhao et al.<sup>9</sup> and extending these findings to macrophages. Given the high percentage of SIRP $\alpha$  v1/v2-heterozygous individuals across human populations (Figure 1), as well as the requirement for full SIRP $\alpha$  antagonism to maximize efficacy, anti-SIRP $\alpha$  antibodies should be capable of antagonizing both SIRP $\alpha$  alleles. Numerous, potent anti-SIRP $\alpha$  antibodies that bind to both human SIRP $\alpha$  alleles are reported in this study.

In addition to the need for pan-allelic antibodies, to facilitate preclinical development, antibodies directed against human SIRP $\alpha$  should be cross-reactive with cynomolgus monkey SIRP $\alpha$  for IND-enabling toxicology studies, and ideally cross-react with mouse SIRP $\alpha$  alleles to avoid the use of surrogates when investigating pharmacology. Only a few anti-human SIRP $\alpha$  antibodies have been described in the scientific literature.<sup>9,16,22,41</sup> These antibodies were raised in mice, and therefore do not cross-react with mouse SIRP $\alpha$ . In order to generate pan-mammalian and pan-allelic anti-SIRP $\alpha$  antibodies, we immunized chickens, which are phylogenetically distinct from mice and humans, thereby increasing the probability of generating a productive antibody response against mouse and human immunogens. Using a multi-species and multi-allele immunization schedule and chickens with wild-type or human Ig repertoires,<sup>30,31</sup> we identified a panel of wild-type, chimeric, or fully human anti-SIRP $\alpha$  blocking and non-blocking antibodies with broad specificities directed against the CD47-binding IgV domain of SIRP $\alpha$ . The isolated antibodies exhibited high-affinity binding to SIRP $\alpha$  with affinities ranging from low nM to low pM, and therefore additional affinity maturation was unnecessary. The panel of antibodies identified displayed broad epitope coverage, enabling the interrogation of the role of epitope on the function of anti-SIRP $\alpha$  antibodies.

The most well-known function of the SIRP $\alpha$ /CD47 interaction is the negative regulation of macrophage phagocytosis. Antibodies that block the interaction between CD47 and SIRP $\alpha$  promote macrophage phagocytosis of tumor cells by inhibiting SIRP $\alpha$  signaling and tipping the balance of pro- and anti-phagocytic signals.<sup>4,9,12,15,16</sup> The anti-SIRP $\alpha$  blocking antibodies described herein potently potentiate macrophage-mediated ADCP of tumor cells, as expected based on the known effects of antagonizing the SIRP $\alpha$ /CD47 axis. Interestingly, we found that non-blocking antibodies directed against SIRP $\alpha$  also enhance macrophage phagocytosis (Figure 7). Enhancement of phagocytosis by non-blocking antibodies was independent of the five different epitopes on the SIRP $\alpha$  IgV-domain that are targeted by the

panel of antibodies we discovered. These data are in agreement with reports by Murata et al.<sup>41</sup> who demonstrated that an anti-SIRPα non-blocking antibody that binds the Ig-C1-like domain of SIRPα also promoted macrophage phagocytosis, albeit to a lower extent than blocking antibodies, suggesting that phagocytosis mediated by non-blocking anti-SIRPα antibodies is not epitope or domain specific, but likely an intrinsic function of antibody-based targeting of SIRPα. Phagocytosis triggered by non-blocking antibodies directed against the SIRPα/CD47 axis appears to be specific to targeting SIRPα, as non-blocking antibodies directed against CD47 have no effect on macrophage phagocytosis.<sup>15</sup> It has been speculated that SIRPα non-blocking antibodies promote phagocytosis through either SIRPα downregulation or the ‘scorpion effect’ where antibody binding to SIRPα permits Fc-domain binding and activation of FcγR signaling on the same cell.<sup>41</sup> However, we observed little to no downregulation of SIRPα during the course of phagocytosis (Fig. S6). Furthermore, the antibodies used in our experiments were mutated to abrogate FcγR and complement binding, ruling out potential contributions of cis-interactions with activating or inhibitory FcγRs. In addition, F(ab')<sub>2</sub> fragments of non-blocking anti-SIRPα antibodies, which lack an Fc domain, were equipotent to their corresponding full-length IgG molecule (Figure 7(c)). The activating receptor SIRPβ has been suggested to be a positive regulator of macrophage phagocytosis,<sup>40</sup> however, the macrophages used in our experiments do not express SIRPβ or SIRPγ (Fig. S8A), therefore anti-SIRP antibody-mediated phagocytosis cannot be attributed to cross-reactivity with SIRPβ or SIRPγ. Collectively, these data suggest that alternative, yet unknown mechanisms are responsible for the potentiation of macrophage phagocytosis by anti-SIRPα antibodies that do not block the interaction with CD47. It is conceivable that antibody binding to SIRPα may restrict CD47-independent SIRPα tonic signaling, thereby promoting phagocytosis. The detailed mechanism by which SIRPα signaling influences macrophage phagocytosis is poorly understood. The broad panel of antibodies described herein may be useful tools to interrogate such biological mechanisms and as promising therapeutics to treat human cancers.

## Materials and Methods

### Bioinformatic analyses of SIRPα polymorphisms

We performed in-depth bioinformatic investigation of IgV domain of the SIRPA gene using sequence data from 1000 Genome Project. For this, we downloaded genomic variants for 2535 sequenced genomes from the Phase 3 dataset present in vcf (variant calling files) from public database (<http://www.internationalgenome.org/data#download>) that span SIRPA gene (chr20:1,875,425–1,920,540, hg18 reference genome). Of 1722 variants in this region, 21 known variants that resulted in missense mutations were present in the IgV domain of the SIRPA gene. Errors in variant calls due to low coverage were fixed by customly written perl script. cDNA sequences of various samples were determined using fixed vcf files and translated to protein sequences by making changes in the consensus coding sequence (CCDS13022.1) of the SIRPA gene using customly written perl script. After which, the translated amino acid sequences in the IgV

domain were then compared with EnsEMBL\_V1 sequence (ENSP00000348307.3).

### Sanger sequencing of selected human samples

Sanger sequencing of 510 samples from different populations were performed (Table S1). These samples were selected from different populations: Mexican Ancestry from Los Angeles USA (MXL), Yoruba in Ibadan, Nigeria (YRI), Utah Residents (CEPH) with Northern and Western European Ancestry (CEU), Colombians from Medellin, Colombia (CLM), British in England and Scotland (GBR), Han Chinese in Beijing, China (CHB), Bengali from Bangladesh (BEB), and Americans of African Ancestry in South West USA (ASW), Japanese in Tokyo, Japan (JPT). DNA samples for these populations were obtained from the NHGRI Sample Repository for Human Genetic Research at the Coriell Institute for Medical Research. DNA was quantified using picogreen assay and normalized to 10 ng/ml. PCR amplification of the target region (exon 3) was carried out using PCR primers pairs forward 5'-TGTCTGGAATACCAGGCTCCCTT and reverse 5'-TACCACCACACCTGATCATTGCTC (IDT Technologies, Iowa City, USA) and KAPA Hyper polymerase (Roche Holding AG, Basel, CH). PCR amplification was performed using the reactions conditions as follows: after preheating at 95°C for 5 min, amplification consisted of 30 cycles at 98°C for 20 s, 68°C for 30 s, and a final extension at 72°C for 5 min. PCR products were purified using the AMPure® XP (Beckmann Coulter, Brea, CA) and quantified using the NanoDrop® (Thermo Fisher Scientific). While performing Sanger sequencing, we noticed the presence of three known deletions (rs138304215-delCT, rs749337996-delCT, and rs139878822-delCGA), and these deletions resulted in chromatograms that are not interpretable. Due to the complexity of these regions, five different Sanger sequencing reactions were performed using the following primers to generate conclusive Sanger sequencing data;

- a) 5'-GGCTCCCTTTCCGGAACCTTCACACAG,
- b) 5'-GTGTGAAGTTCCGAAAGGGAGCCCCGAT,
- c) 5'-GCTCCAGACTTAAACTCCACGTCATCGG,
- d) 5'-CCTGCTCCAGACTTAAACTCCACGTCAG and
- e) 5'-GTGTGAAGTTCCGAAAGGGAGCCCT.

DNA (10 ng) was sequenced using the BigDye Terminator® cycle sequencing kit (v3.1; Thermo Fisher Scientific). Following purification using the Centri-Sep® Spin Columns (Thermo Fisher Scientific), the nucleotide sequences were determined using an ABI3730XL Genetic Analyzer (Thermo Fisher Scientific). Sequence data were aligned using Sequencher® DNA sequence analysis software (v5.2.4; Gene Codes Corporation, Ann Arbor, MI). All the Sanger sequencing results (Table S1) were found to be concordant with our bioinformatic analysis.

### Generation of antigens for immunization and screening

The IgV domains of SIRPα antigens from four respective sources were generated for immunization as fusion to human IgG-Fc to increase immunogenicity. Specifically, they are human SIRPα v1 (NP\_542970.1), SIRPα v2 (CAA71403.1),

mouse 129 SIRP $\alpha$  (162330193) and NOD SIRP $\alpha$  sequence as described in references<sup>42,43</sup> and reported in Figure S2 and Figure S3. The Fc-fused proteins were expressed in Expi293 cells (Invitrogen) using standard manufacturer's protocol. Expression cultures were typically grown for five days at 37°C in 8% CO<sub>2</sub>. Supernatants were harvested via centrifugation and sterile filtered. Proteins were affinity purified using MabSelect Sure LX resin (GE Healthcare). For SPR screening, the IgV domains of the respective SIRP were expressed in Expi293 cells as described above as either His-tagged or His-Avi-tagged fusions and purified using Ni-Sepharose 6 Fast Flow affinity purification (GE Healthcare). The panel of SIRP generated for SPR screening were the IgV domain from human SIRP $\alpha$  v1 (NP\_542970.1), human SIRP $\alpha$  v2 (CAA71403.1), cynomolgus SIRP $\alpha$  (EHH65484.1), mouse 129 SIRP $\alpha$  (162330193), NOD/BALBc/C57BL/6 SIRP $\alpha$  (sequences as described in references 41 and 42 and reported in Figure S2 and Figure S3), and human SIRP $\gamma$  (NP\_061026.2) and human SIRP $\beta$ 1 (NP\_006056.2) (sequences as reported in Figure S4). The IgV domain of CD47 was generated as described in reference 12. The high-affinity SIRP $\alpha$  variant CV1 was generated as described in reference 14.

### Immunization of chickens

In total, 19 chickens were immunized. Specifically, these include four wildtype White Leghorn chickens, 4 SynVH chickens, which are transgenic chickens containing VH from human and VL from chicken,<sup>31</sup> and 11 chickens with fully human immunoglobulin loci called OmniChicken.<sup>30</sup> The chickens were immunized with varied schedules having alternating doses and boosts of human SIRP $\alpha$  v1, human SIRP $\alpha$  v2 and mouse SIRP $\alpha$  (m129 or NOD). The immunization protocol was approved by the Institutional Animal Care and Use Committee. Sera were collected bi-weekly during the immunization to determine plasma titer by ELISA. In total, eight immunized birds with good final titers were selected for preparation of splenocytes and lymphocyte screenings using the GEM assay (Figure 2(b)). The immunization schemes for the selected birds are described in Table 2. For example, wildtype 21,288 bird was initially immunized with 100  $\mu$ g human SIRP $\alpha$  v1 at week 1, boost with 50  $\mu$ g of human SIRP $\alpha$  v2 at week 3, draw at week 4, boost with 50  $\mu$ g of human SIRP $\alpha$  v1 at week 5, draw at week 6, boost with 50  $\mu$ g of human SIRP $\alpha$  v2 at week 7, and draw at week 8.

### Screening single B cells using the GEM assay

A single lymphocyte screening and recovery method, the GEM assay was used to isolate antigen-specific mAbs from immunized chicken. The GEM assay involves placing single mAb-secreting lymphocytes in proximity with reporter beads. The secreted mAb diffuses locally within the GEM and has the opportunity to bind to the reporter beads. Bound mAb is detected directly through the use of a fluorescent secondary mAb, anti-IgY Alexa 594 (Life Technologies A-11042). There were four beads used in this program: 1) a 5  $\mu$ m latex bead coated with hSIRP $\alpha$  v1; 2) a 5  $\mu$ m blue latex bead coated with mSIRP $\alpha$  (129, NOD or BALBc); 3) a 1.4  $\mu$ m latex bead coated with hSIRP $\alpha$  v2, and 4) a 5  $\mu$ m latex bead coated with CD47

followed by a mixture of high-affinity SIRP $\alpha$  v1 and v2. Three of the four beads were encapsulated with a single B cell from the chicken being screened depending on the objective of the screen. For example, if the goal of the screen was to ensure species cross-reactivity, then the beads encapsulated were 5  $\mu$ m hSIRP $\alpha$  v1, 1.4  $\mu$ m hSIRP $\alpha$  v2 and 5  $\mu$ m blue mSIRP $\alpha$ . Fresh beads were coated within a week of performing GEM assays. To coat beads, protein was diluted in phosphate-buffered saline (PBS). The diluted protein was added directly to the beads and incubated at 4°C overnight while rocking. Beads were washed with PBS and blocked with 3% filtered milk in PBS. Beads were washed and tested using reactive plasma from immunized chickens. GEMs were viewed on a Leica DMI 6000 B inverted fluorescent microscope.

### Cloning and expression of recombinant mAbs

Cells secreting antigen-specific mAbs were isolated from the GEM assay, and their respective V genes were amplified by a two-step, semi-nested strategy as described.<sup>32</sup> Briefly, the V-genes were cloned through RT PCR and cloned into the mammalian expression vector pF5a (Promega) in scFv-Fc format (IgG1-Fc isotype with effector attenuating Fc substitutions<sup>37,38,44</sup> that ablate Fc $\gamma$ R and complement binding). Plasmids containing recombinant scFv-Fc from the GEM harvests were transiently transfected into HEK293F (Thermo Fisher) and clonal supernatants were harvested. Supernatants were tested for binding activity by SPR described below. All clones that were confirmed as binding their respective targets were fully sequenced to avoid redundancies. Select clones were converted to full-length IgG1 molecules with effector attenuating Fc substitutions and produced in HEK293F.

### SPR Screening of Antibody Clones

Binding of the antibody clones to various SIRP proteins was determined using SPR detection on a ProteOn XPR36 instrument (Bio-Rad, Hercules, CA) using PBS (pH 7.4) supplemented with 0.01% Tween-20 (PBS-T) as running buffer. The pre-filtered media containing the recombinant scFv-Fc were used directly for the assay. First, anti-human IgG Fc (BR-1008-39, GE Healthcare) was amine-coupled onto a GLC sensor chip (Bio-Rad, Cat. #1765011) to generate the capture surfaces for the antibodies. About 4000 RU per flow cell of immobilized anti-human IgG Fc is achieved. Each clone was screened using the same method as follows: 5–10  $\mu$ L of pre-filtered media in 10 mM sodium acetate buffer (pH 4.5) was injected for 2 min at 30  $\mu$ L/min; buffer flow for 1 min at 100  $\mu$ L/min; SIRP analyte (100 nM) injected for 1 min at 100  $\mu$ L/min, followed by a dissociation cycle of 10 min; regeneration of chip surface by flowing 3 M magnesium chloride for 1 min at 25  $\mu$ L/min in both orientation; and buffer flow for 1 min at 100  $\mu$ L/min. Biosensor data were double-referenced by subtracting the interspot data (containing no immobilized anti-human IgG Fc) from the reaction spot data (immobilized anti-human IgG Fc), and then subtracting the response of a buffer "blank" analyte injection from that of an analyte injection. Binding was fitted using a 1:1 Langmuir and  $k_{\text{off}}$  (1/s) values calculated. All SPR assays were performed at 25°C and all SPR assays described here used PBS-T as running buffer.

### Anti-SIRP $\alpha$ antibody screen to identify effect on the SIRP $\alpha$ /CD47 interaction

To assess if antibodies can block binding of SIRP $\alpha$  to CD47, an SPR screen was carried out. Antibody capture was carried out using an anti-human IgG-Fc immobilized GLC surface prepared as described above. A SIRP $\alpha$  variant (CV1) engineered to bind CD47 with high nM affinity<sup>14</sup> was used for the screen rather than a wildtype SIRP $\alpha$ . This is because the wildtype SIRP $\alpha$  variant has low  $\mu$ M binding affinity to CD47, which does not allow stable complex interaction to assess sandwich formation. First, approximately 5–10  $\mu$ L of pre-filtered media containing the antibodies in 10 mM sodium acetate buffer (pH 4.5) was injected for 2 min at 30  $\mu$ L/min and captured over the anti-human IgG-Fc immobilized GLC surface followed by a brief buffer flow of 1 min at 100  $\mu$ L/min. Next, 100 nM of a high-affinity SIRP $\alpha$  variant (CV1) pre-mixed with CD47 at different concentrations of 0, 20, 55, 500, or 1500 nM was injected separately for a minute at 100  $\mu$ L/min with a dissociation time for 10 min.

### Epitope binning

Epitope binning was carried out using a classical sandwich approach using methods described by Abdiche et al.<sup>34</sup> An anti-SIRP $\alpha$  antibody was first immobilized on a GLC chip, and then human SIRP $\alpha$  v1 was injected followed by a second anti-SIRP $\alpha$  antibody. If the second antibody was able to bind the complex formed between the first anti-SIRP $\alpha$  antibody and SIRP $\alpha$ , the first and second antibodies were determined to bind different epitopes. If the second antibody was not able to bind, the first and second antibodies were determined to share an epitope. The detailed components of the experiment are described as follows. First, anti-SIRP $\alpha$  antibodies were immobilized on GLC chips using Proteon Amine Coupling Kit as described before. Briefly, for the immobilization step, GLC chip was activated with 1-ethyl-3-(3-dimethylaminopropyl) carbodiimide hydrochloride (EDAC)/sulfo-N-hydroxysuccinimide (Sulpho-NHS) 1:1 (Biorad) diluted 1/80 for 300 s at 25  $\mu$ L/min. Anti-SIRP $\alpha$  antibodies were diluted to 80 nM concentration in 10 mM sodium acetate buffer pH 4.5 and immobilized to the chip at 30  $\mu$ L/min for 50 s. The chip was inactivated with ethanolamine for 300 s at 25  $\mu$ L/min. After which, the IgV domain of SIRP $\alpha$  v1 (100 nM) was first injected at 100  $\mu$ L/min for 60 s, followed by injection of the anti-SIRP $\alpha$  antibodies in testing (100–150 nM) at 100  $\mu$ L/min for 60 s. The surfaces were regenerated with a 2:1 v/v blend of Pierce IgG elution buffer/4 M NaCl. The resulting sensorgrams were used to score and group the antibodies into different bins according to their binding profiles.

### Determination of $K_D$

The binding affinities of anti-SIRP $\alpha$  antibodies to SIRP $\alpha$  from various species (human v1, human v2, cynomolgus, mouse 129, BL6, BALBc, NOD), SIRP $\beta$ 1 and SIRP $\gamma$  were determined using direct immobilization of the antibodies (via GLC chip). All analytes were used at their nominal concentrations determined by A280 absorbance and molar extinction coefficient. Analytes were injected in a “one-shot” kinetic mode<sup>45</sup> and flowed over anti-SIRP $\alpha$  antibodies immobilized (~1000 RUs) on GLC chips using

ProteOn Amine Coupling Kit. For the immobilization step, GLC chip was activated with EDAC/Sulpho-NHS 1:1 (Biorad) diluted 1/100 for 300 s at 25  $\mu$ L/min. Anti-SIRP $\alpha$  antibodies were diluted to 80 nM concentration in 10 mM sodium acetate buffer pH 4.5 and immobilized to the chip at 30  $\mu$ L/min for 50 s. Chip was inactivated with ethanolamine for 300 s at 25  $\mu$ L/min. The analytes (e.g., SIRP $\alpha$  from different species, SIRP $\beta$ 1, SIRP $\gamma$ ) were injected in a “one-shot” kinetic mode at nominal concentrations of 100, 33, 11, 3.7, 1.2 and 0 nM. Association times were monitored for 90 s at 100  $\mu$ L/min, and dissociation times were monitored for 1200 s. The surfaces were regenerated with a 2:1 v/v blend of Pierce IgG elution buffer/4M NaCl. Biosensor data were double-referenced by subtracting the interspot data (containing no immobilized protein) from the reaction spot data (immobilized protein), and then subtracting the response of a buffer “blank” analyte injection from that of an analyte injection. Double-referenced data were fit globally to a simple Langmuir model, and the  $K_D$  value was calculated from the ratio of the apparent kinetic rate constants ( $K_D = k_d/k_a$ ).

### Crystallization of anti-SIRP $\alpha$ Fab: SIRP $\alpha$ complexes

The IgV domain of SIRP $\alpha$  v1 was generated for crystallography as previously described.<sup>46</sup> A mutation N80A was introduced to produce a homogenous and non-glycosylated SIRP $\alpha$  v1 that would be most amenable for crystallization. The anti-SIRP $\alpha$  antibodies were generated as Fab fragments with a 6His-tag at the C-terminus of the truncated hinge domain. Both SIRP $\alpha$  v1 and the Fab fragments were expressed in Expi293 and purified using Ni-Sepharose 6 Fast Flow affinity purification (GE Healthcare) followed by gel filtration. The Fabs and SIRP $\alpha$  v1 proteins were purified individually prior to being complexed (with SIRP $\alpha$  v1 in molar excess) proceeded by a final SEC step to separate unbound proteins. The final formulation buffer is minimal with 10 mM Tris pH 7.5 and 50 mM NaCl. The purified Fabs and SIRP $\alpha$  complex sample is stable at 4°C and was concentrated to 10–12 mg/mL for crystallography.

The methods for the anti-SIRP $\alpha$  antibodies and SIRP $\alpha$  complex structure solution followed well-established principles of crystallography, beginning with sparse matrix crystallization trials. Conditions were selected from initial trials and optimized for formation of favorable crystals for harvest and synchrotron X-ray diffraction screening. Once a crystallization regime is established for one complex, the protocol can be followed for subsequent anti-SIRP $\alpha$  Fab antibodies: SIRP $\alpha$  complexes. Crystallization experiments used the sitting drop vapor diffusion technique for the initial sparse matrix screening and commercially available kits from Qiagen. Crystallization trials were set in varying ratios ranged in 1:1, 2:1, and 3:1 of anti-SIRP $\alpha$  Fab: SIRP $\alpha$  complex to crystallant in total volume of 1  $\mu$ L in the subwells of the 96-well (8 x 12) tray while 100  $\mu$ L of crystallization solution was placed in the well reservoir. The completed plates were sealed to allow vapor diffusion to occur and stored in a 12°C incubator. Crystallization of the five anti-SIRP $\alpha$  Fab: SIRP $\alpha$  complexes were achieved with derivatives of two main conditions as shown in Table S5. The detailed steps involved for crystal harvest, data collection, and processing, structure building and refinement are described in

the supplementary materials. The PDB codes for the structures generated are 6NMV, 6NMU, 6NMT, 6NMS, and 6NMR.

### **Epitope mapping and superimposition analysis based on crystal structures**

Buried surface area of the antigen for the epitope was calculated as the difference between the solvent-accessible surface area of the antigen alone and antigen in complex with the Fab fragment of the antibody. The accessible surface area was calculated by the rolling ball method<sup>47,48</sup> with a probe radius of 1.4 Å. Buried surface area is reported in Å<sup>2</sup> (Table S3). All Fab antibody: SIRPα complexes were aligned by superimposing the carbon atoms of SIRPα from each structure with the CD47: SIRPα complex (v1 variant) structure (PDB: 4CMM).<sup>49</sup> Superimposition was performed using PYMOL. The calculated RMSD (0.50) between the aligned SIRPα structures in the complexes showed little variation, hence validating the overlay (Table S6). Therefore, the alignment of the SIRPα structures is credible to establish a reference point to analyze the varying binding epitopes of the Fab anti-SIRPα antibodies.

### **Cell staining to determine binding profiles of anti-SIRP antibodies**

Peripheral blood mononuclear cells (PBMCs) were isolated from Trima residuals of healthy individuals (purchased from Vitalent) with Ficoll-Paque Plus (GE Cat. 17144003). CD14+ monocytes were isolated from PBMC by negative selection (Miltenyi Cat. 130-091-153) per manufacturer's protocol. Monocyte-derived macrophages (MDM $\phi$ ) were differentiated from CD14+ monocytes using macrophage colony-stimulating factor (M-CSF) (Miltenyi Cat. 130-096-491) (50 ng/mL) for 9 days in culture medium. Cells were stained with FcR block (Miltenyi Cat. 130-059-901) in PBS (Gibco Cat. 10010-031) + 0.5% bovine serum albumin (BSA) (Sigma A1933) with the addition of the following monoclonal antibodies (all from Biolegend): PerCP-Cy5.5-labeled CD3 (Cat. 317336); AF488-labeled CD4 (Cat. 344618); BV510-labeled CD8 (Cat. 344732); PE-CY7-labeled CD14 (Cat. 325618); PE-labeled LSB2.20 (Cat. 336606), B4B6 (Cat. 323906) and matched isotype control (Cat. 400112). Purified anti-SIRP antibodies discovered in house and un-labeled LSB2.20 and SE5A5 (Biolegend Cat. 336602 and Cat. 323802) were amine-labeled with Alexa Fluor 647 (ThermoScientific Cat. A20173). Fixable viability dye (eBioscience Cat. 65-0865-14) was used to identify live cells. Samples were acquired with Canto II flow cytometer (BD) and analyzed using FlowJo software.

### **Macrophage-mediated antibody-dependent cellular phagocytosis assay**

CD14+ cells were purified from Trima residuals (Blood Centers of the Pacific) with Ficoll-Paque Plus and negative selection (Monocyte Isolation Kit II, Miltenyi Biotec) according to the manufacturers' protocols. MDM $\square$  were made by seeding six million CD14+ cells into 150 mm tissue culture dishes (Corning) in growth medium supplemented with 10% fetal bovine serum (Millipore) and 50 ng/mL M-CSF

(Miltenyi Biotec). Cells were cultured for 7 to 11 days. Adherent cells were detached from culture plates with TrypLE Select (Thermo Fisher Scientific). Target cells were labeled with the Celltrace CFSE Cell Proliferation kit (Thermo Fisher Scientific) according to the manufacturer's instructions. 100,000 target cells and 50,000 monocyte-derived macrophages were incubated in ultra-low attachment U-bottom 96-well plates (Corning) with anti-SIRP antibodies and the corresponding tumor-specific antibody for 2 h at 37° C. Cetuximab was added at a concentration of 0.01–0.1 µg/ml for DLD-1 cells and trastuzumab was added at a concentration of 0.01 µg/ml for OE19 cells. F(ab')<sub>2</sub> fragments were prepared using the Pierce F(ab')<sub>2</sub> purification kit following the manufactures recommended protocol (ThermoFisher) and undigested IgG was purified away from F(ab')<sub>2</sub> fragments via Protein A. Cetuximab and trastuzumab were produced in HEK293F using standard monoclonal antibody production methods. Sequences were obtained from the Drugbank ([www.drugbank.ca](http://www.drugbank.ca)), DB00072 and DB00002 for trastuzumab and cetuximab, respectively.

For flow cytometry, cells were incubated in human FcR Blocking Reagent (Miltenyi Biotec) and stained with fluorochrome-labeled antibodies against CD33 (clone WM53, Biolegend) and CD206 (clone 15-2, Biolegend). To eliminate macrophage/target cell adhesion from analyses, antibody against CD326 (clone 9C4, Biolegend) was included for DLD-1 and OE19 cells. Furthermore, a pulse geometry gate of forward scatter signal area vs height was used to select for single cells. Fixable viability dye (Thermo Fisher Scientific) was used to identify live cells. Cells were analyzed on a FACS Canto II flow cytometer (BD Biosciences) with subsequent analysis using FlowJo software. Percent phagocytosis indicates the percentage of viable CD33+ CD206+ macrophages that stain negative for CD326 and positive for CFSE. When applicable, four parameter fit curves were generated with Prism 7 software (GraphPad).

### **Cell-based SIRPα antagonism assay**







Antagonism of CD47 binding by anti-SIRPα antibodies was performed using CD47-Fc fluorescently labeled using the Alexa Fluor 647 Protein Labeling Kit (Thermo Fisher Scientific) according to the manufacturer's instructions. Alexa Fluor 647-labeled CD47-Fc at a concentration of 250 nM and fluorescently labeled anti-CD14 (Biolegend Cat. 325618) were added to 100,000 PBMCs in 100 µL volume of FACs buffer (PBS + 0.5% BSA) supplemented with a cocktail of human Fc block (Miltenyi Biotec). After 30 min on ice, cells were washed once in staining buffer. Anti-SIRPα was added at a concentration of 1.25 µM with 10-fold serial dilutions. After 30 min on ice, cells were washed twice in staining buffer and fixed in 0.5% paraformaldehyde. Cells were analyzed using a FACS Canto II (BD Biosciences), with subsequent data analysis and histogram plotting using FlowJo 10.7 and Prism 7 software (GraphPad).

### **Disclosure statement**

These studies were sponsored by ALX Oncology. JS, JTS, ES, LD, OH, SEK, AC, TCK, HW, and JP are all employed by ALX Oncology and are

shareholders. The funder provided support in the form of salaries but did not have any additional role in the study design, data collection, and analysis, decision to publish, or preparation of the manuscript.

## ORCID

Janet Sim  <http://orcid.org/0000-0002-6438-1995>  
 Jonathan T. Sockolosky  <http://orcid.org/0000-0002-5441-1409>  
 Emma Sangalang  <http://orcid.org/0000-0002-6222-6588>  
 Ardian S. Wibowo  <http://orcid.org/0000-0002-0955-8903>  
 Josh Carter  <http://orcid.org/0000-0001-7322-349X>  
 Anup Madan  <http://orcid.org/0000-0002-0967-7574>  
 Laura Doyle  <http://orcid.org/0000-0003-1241-7017>  
 Steven E. Kauder  <http://orcid.org/0000-0003-4853-6544>  
 Tracy C. Kuo  <http://orcid.org/0000-0001-6297-8694>  
 Hong Wan  <http://orcid.org/0000-0003-2537-8950>  
 Jaume Pons  <http://orcid.org/0000-0002-0831-419X>

## References

- Sharma P, Allison JP. Immune checkpoint targeting in cancer therapy: toward combination strategies with curative potential. *Cell*. 2015;161(2):205–14. doi:10.1016/j.cell.2015.03.030.
- Ribas A, Wolchok JD. Cancer immunotherapy using checkpoint blockade. *Science*. 2018;359(6382):1350–55. doi:10.1126/science.aar4060.
- Moynihan KD, Irvine DJ. Roles for innate immunity in combination immunotherapies. *Cancer Res*. 2017;77(19):5215–21. doi:10.1158/0008-5472.CAN-17-1340.
- Ho CCM, Guo N, Sockolosky JT, Ring AM, Weiskopf K, Özkan E, Mori Y, Weissman IL, Garcia KC. “Velcro” engineering of high affinity CD47 ectodomain as signal regulatory protein  $\alpha$  (SIRP $\alpha$ ) antagonists that enhance antibody-dependent cellular phagocytosis. *J Biol Chem*. 2015;290(20):12650–63. doi:10.1074/jbc.M115.648220.
- Barclay AN, Van Den Berg TK. The interaction between signal regulatory protein alpha (SIRP $\alpha$ ) and CD47: structure, function, and therapeutic target. *Annu Rev Immunol*. 2014;32:25–50. doi:10.1146/annurev-immunol-032713-120142.
- Willingham SB, Volkmer J-P, Gentles AJ, Sahoo D, Dalerba P, Mitra SS, Wang J, Contreras-Trujillo H, Martin R, Cohen JD, et al. The CD47-signal regulatory protein alpha (SIRP $\alpha$ ) interaction is a therapeutic target for human solid tumors. *Proc Natl Acad Sci*. 2012;109(17):6662–67. doi:10.1073/pnas.1121623109.
- Lange J, Skaletsky H, van Daalen SKM, Embry SL, Korver CM, Brown LG, Oates RD, Silber S, Repping S, Page DC. Isodicentric Y chromosomes and sex disorders as byproducts of homologous recombination that maintains palindromes. *Cell*. 2009;138(5):855–69. doi:10.1016/j.cell.2009.07.042.
- Sockolosky JT, Dougan M, Ingram JR, Ho CCM, Kauke MJ, Almo SC, Ploegh HL, Garcia KC. Durable antitumor responses to CD47 blockade require adaptive immune stimulation. *Proc Natl Acad Sci U S A*. 2016;113(19):E2646–E2654. doi:10.1073/pnas.1604268113.
- Ge C, Du J, Zhao, L, Wang L, Liu Y, Li D, Yang Y, Zhou R, Zhao Y, Chai Z, et al. Binding of blood proteins to carbon nanotubes reduces cytotoxicity. *Proc Natl Acad Sci U S A*. 2011;108(41):16968–7. doi:10.1073/pnas.1105270108.
- Tseng D, Volkmer J-P, Willingham SB, Contreras-Trujillo H, Fathman JW, Fernhoff NB, Seita J, Inlay MA, Weiskopf K, Miyanishi M, et al. Anti-CD47 antibody-mediated phagocytosis of cancer by macrophages primes an effective antitumor T-cell response. *Proc Natl Acad Sci*. 2013;110(27):11103–08. doi:10.1073/pnas.1305569110.
- Liu X, Pu Y, Cron K, Deng L, Kline J, Frazier WA, Xu H, Peng H, Fu Y-X, Xu MM. CD47 blockade triggers T cell-mediated destruction of immunogenic tumors. *Nat Med*. 2015;21(10):1209–15. doi:10.1038/nm.3931.
- Kauder SE, Kuo TC, Harrabi O, Chen A, Sangalang E, Doyle L, Rocha SS, Bollini S, Han B, Sim J, et al. ALX148 blocks CD47 and enhances innate and adaptive antitumor immunity with a favorable safety profile. *PLoS One*. 2018;13(8):e0201832. doi:10.1371/journal.pone.0201832.
- Eiring AM, Page BDG, Kraft IL, Mason CC, Vellore NA, Resetca D, Zabriskie MS, Zhang TY, Khorashad JS, Engar AJ, et al. Combined STAT3 and BCR-ABL1 inhibition induces synthetic lethality in therapy-resistant chronic myeloid leukemia. *Leukemia*. 2017;31(5):1253–54. doi:10.1038/leu.2017.14.
- Weiskopf K, Ring AM, Ho CCM, Volkmer J-P, Levin AM, Volkmer AK, Özkan E, Fernhoff NB, van de Rijn M, Weissman IL, et al. Engineered SIRP $\alpha$  variants as immunotherapeutic adjuvants to anticancer antibodies. *Science*. 2013;341(6141):88–91. doi:10.1126/science.1238856.
- Chao MP, Alizadeh AA, Tang C, Myklebust JH, Varghese B, Gill S, Jan M, Cha AC, Chan CK, Tan BT, et al. Anti-CD47 antibody synergizes with rituximab to promote phagocytosis and eradicate non-Hodgkin lymphoma. *Cell*. 2010;142(5):699–713. doi:10.1016/j.cell.2010.07.044.
- Ring NG, Herndler-Brandstetter D, Weiskopf K, Shan L, Volkmer J-P, George BM, Lietzenmayer M, McKenna KM, Naik TJ, McCarty A, et al.; Ring NG, et al. Anti-SIRP $\alpha$  antibody immunotherapy enhances neutrophil and macrophage antitumor activity. *Proc Natl Acad Sci U S A*. 2017;114(49):E10578–E10585. doi:10.1073/pnas.1710877114.
- Weiskopf K. Cancer immunotherapy targeting the CD47/SIRP $\alpha$  axis. *Eur J Cancer*. 2017;76:100–09. doi:10.1016/j.ejca.2017.02.013.
- Advani R, Flinn I, Popplewell L, Forero A, Bartlett NL, Ghosh N, Kline J, Roschewski M, LaCasce A, Collins GP, et al. CD47 Blockade by Hu5F9-G4 and rituximab in non-Hodgkin’s lymphoma. *N Engl J Med*. 2018;379(18):1711–21. doi:10.1056/NEJMoa1807315.
- Lakhani N, LoRusso P, Chow LQ, Bang Y, Gainor J, Lee J, Chung H, Lee K, Hodi S, Fanning P, et al. A phase 1 study of ALX148: CD47 blockade in combination with anticancer antibodies to bridge innate and adaptive immune responses for advanced malignancy [abstract]. Proceedings of the 33rd Annual Meeting of the Society for Immunotherapy of Cancer; 2018 Nov 7-11; Washington, DC, p Abstract nr P335.
- Ingram JR, Blomberg OS, Sockolosky JT, Ali L, Schmidt FI, Pishesha N, Espinosa C, Dougan SK, Garcia KC, Ploegh HL, et al. Localized CD47 blockade enhances immunotherapy for murine melanoma. *Proc Natl Acad Sci U S A*. 2017;114(38):10184–89. doi:10.1073/pnas.1710776114.
- Liu J, Wang L, Zhao F, Tseng S, Narayanan C, Shura L, Willingham S, Howard M, Prohaska S, Volkmer J, et al. Pre-clinical development of a humanized anti-CD47 antibody with anti-cancer therapeutic potential. *PLoS One*. 2015;10(9):e0137345. doi:10.1371/journal.pone.0137345.
- Vernet M-A, Reynard S, Fizez A, Schaeffer J, Pannetier D, Guedj J, Rives M, Georges N, Garcia-Bonnet N, Sylla AI, et al. Clinical, virological, and biological parameters associated with outcomes of Ebola virus infection in Macenta, Guinea. *JCI Insight*. 2017;2(6):e89140. doi:10.1172/jci.insight.88864.
- Matlung HL, Szilagyi K, Barclay NA, van Den Berg TK. The CD47-SIRP $\alpha$  signaling axis as an innate immune checkpoint in cancer. *Immunol Rev*. 2017;276(1):145–64. doi:10.1111/imr.2017.276.issue-1.
- Takenaka K, Prasolava TK, Wang JCY, Mortin-Toth SM, Khalouei S, Gan OI, Dick JE, Danska JS. Polymorphism in Sirpa modulates engraftment of human hematopoietic stem cells. *Nat Immunol*. 2007;8(12):1313–23. doi:10.1038/ni1527.
- Treffers LW, Zhao XW, van der Heijden J, Nagelkerke SQ, van Rees DJ, Gonzalez P, Geissler J, Verkuijlen P, van Houdt M, de Boer M, et al. Genetic variation of human neutrophil Fc $\gamma$  receptors and SIRP $\alpha$  in antibody-dependent cellular cytotoxicity towards cancer cells. *Eur J Immunol*. 2018;48(2):344–54. doi:10.1002/eji.201747215.
- Sudmant PH, Rausch T, Gardner EJ, Handsaker RE, Abyzov A, Huddleston J, Zhang Y, Ye K, Jun G, Hsi-Yang Fritz M, et al. An integrated map of structural variation in 2,504 human



- genomes. *Nature*. 2015;526(7571):75–81. doi:10.1038/nature15394.
27. O'Leary MA, Bloch JJ, Flynn JJ, Gaudin TJ, Giallombardo A, Giannini NP, Goldberg SL, Kraatz BP, Luo Z-X, Meng J, et al. The placental mammal ancestor and the post-K-Pg radiation of placentals. *Science*. 2013;339(6120):662–67. doi:10.1126/science.1229237.
  28. Dodgson JB, Delany ME, Cheng HH. Poultry genome sequences: progress and outstanding challenges. *Cytogenet Genome Res*. 2011;134(1):19–26. doi:10.1159/000324413.
  29. Desoubieux G, Reichert JM, Sleeman M, Reckamp KL, Ryffel B, Adamczewski JP, Sweeney TD, Vanbever R, Diot P, Owen CA, et al. Therapeutic monoclonal antibodies for respiratory diseases: current challenges and perspectives, March 31 - April 1, 2016, Tours, France. *MAbs*. 2016;8(6):999–1009. doi:10.1080/19420862.2016.1196521.
  30. Ching KH, Collarini EJ, Abdiche YN, Bedinger D, Pedersen D, Izquierdo S, Harriman R, Zhu L, Etches RJ, van de Lavoie M-C, et al. Chickens with humanized immunoglobulin genes generate antibodies with high affinity and broad epitope coverage to conserved targets. *MAbs*. 2018;10(1):71–80. doi:10.1080/19420862.2017.1386825.
  31. Schusser B, Collarini EJ, Pedersen D, Yi H, Ching K, Izquierdo S, Thoma T, Lettmann S, Kaspers B, Etches RJ, et al. Expression of heavy chain-only antibodies can support B-cell development in light chain knockout chickens. *Eur J Immunol*. 2016;46(9):2137–48. doi:10.1002/eji.201546171.
  32. Mettler Izquierdo S, Varela S, Park M, Collarini EJ, Lu D, Pramanick S, Rucker J, Lopalco L, Etches R, Harriman W. High-efficiency antibody discovery achieved with multiplexed microscopy. *Microscopy*. 2016;65(4):341–52. doi:10.1093/jmicro/dfw014.
  33. Abdiche YN, Yeung AY, Ni I, Stone D, Miles A, Morishige W, Rossi A, Strop P, Mantis NJ. Antibodies targeting closely adjacent or minimally overlapping epitopes can displace one another. *PLoS One*. 2017;12(1):e0169535. doi:10.1371/journal.pone.0169535.
  34. Abdiche YN, Miles A, Eckman J, Foletti D, Van Blarcom TJ, Yeung YA, Pons J, Rajpal A, Dübel S. High-throughput epitope binning assays on label-free array-based biosensors can yield exquisite epitope discrimination that facilitates the selection of monoclonal antibodies with functional activity. *PLoS One*. 2014;9(3):e92451. doi:10.1371/journal.pone.0092451.
  35. Hatherley D, Graham SC, Turner J, Harlos K, Stuart DI, Barclay AN. Paired receptor specificity explained by structures of signal regulatory proteins alone and complexed with CD47. *Mol Cell*. 2008;31(2):266–77. doi:10.1016/j.molcel.2008.05.026.
  36. Spangler JB, Tomala J, Luca V, Jude K, Dong S, Ring A, Votavova P, Pepper M, Kovar M, Garcia K. Antibodies to interleukin-2 elicit selective T cell subset potentiation through distinct conformational mechanisms. *Immunity*. 2015;42(5):815–25. doi:10.1016/j.immuni.2015.04.015.
  37. Lo M, Kim HS, Tong RK, Bainbridge TW, Vernes J-M, Zhang Y, Lin YL, Chung S, Dennis MS, Zuchero YJY, et al. Effector-attenuating substitutions that maintain antibody stability and reduce toxicity in mice. *J Biol Chem*. 2017;292(9):3900–08. doi:10.1074/jbc.M116.767749.
  38. Shields RL, Namenuk AK, Hong K, Meng YG, Rae J, Briggs J, Xie D, Lai J, Stadlen A, Li B, et al. High Resolution Mapping of the Binding Site on Human IgG1 for FcγRI, FcγRII, FcγRIII, and FcRn and Design of IgG1 Variants with Improved Binding to the FcγR. *J Biol Chem*. 2001;276(9):6591–604. doi:10.1074/jbc.M009483200.
  39. Poirier N, Mary C, Vanhove B, Gauttier V, Thepenier V, Pengam S. International Patent Publication WO2017178653A3. New anti-SIRPa antibodies and their therapeutic applications. 2017.
  40. Hayashi A, Ohnishi H, Okazawa H, Nakazawa S, Ikeda H, Motegi S-I, Aoki N, Kimura S, Mikuni M, Matozaki T. Positive regulation of phagocytosis by SIRPβ and its signaling mechanism in macrophages. *J Biol Chem*. 2004;279(28):29450–60. doi:10.1074/jbc.M400950200.
  41. Murata Y, Tanaka D, Hazama D, Yanagita T, Saito Y, Kotani T, Oldenborg P-A, Matozaki T. Anti-human SIRPa antibody is a new tool for cancer immunotherapy. *Cancer Sci*. 2018;109(5):1300–08. doi:10.1111/cas.2018.109.issue-5.
  42. Kasaian MT, Page KM, Fish S, Brennan A, Cook TA, Moreira K, Zhang M, Jesson M, Marquette K, Agostinelli R, et al. Therapeutic activity of an interleukin-4/interleukin-13 dual antagonist on oxazolone-induced colitis in mice. *Immunology*. 2014;143(3):416–17. doi:10.1111/imm.12319.
  43. Iwamoto C, Takenaka K, Urata S, Yamauchi T, Shima T, Kuriyama T, Daitoku S, Saito Y, Miyamoto T, Iwasaki H, et al. The BALB/c-specific polymorphic SIRPA enhances its affinity for human CD47, inhibiting phagocytosis against human cells to promote xenogeneic engraftment. *Exp Hematol*. 2014;42(3):163–171.e1. doi:10.1016/j.exphem.2013.11.005.
  44. Xu D, Alegre M-L, Varga SS, Rothermel AL, Collins AM, Pulito VL, Hanna LS, Dolan KP, Parren PWI, Bluestone JA, et al. In Vitro Characterization of five humanized OKT3 effector function variant antibodies. *Cell Immunol*. 2000;200(1):16–26. doi:10.1006/cimm.2000.1617.
  45. Bravman T, Bronner V, Lavie K, Notcovich A, Papalia GA, Myszycka DG. Exploring “one-shot” kinetics and small molecule analysis using the ProteOn XPR36 array biosensor. *Anal Biochem*. 2006;358(2):281–88. doi:10.1016/j.ab.2006.08.005.
  46. Hatherley D, Lea SM, Johnson S, Barclay AN. Polymorphisms in the human inhibitory signal-regulatory protein α do not affect binding to its ligand CD47. *J Biol Chem*. 2014;289(14):10024–28. doi:10.1074/jbc.M114.550558.
  47. Shrake A, Rupley JA. Environment and exposure to solvent of protein atoms. Lysozyme and insulin. *J Mol Biol*. 1973;79(2):351–71. doi:10.1016/0022-2836(73)90011-9.
  48. Hasel W, Hendrickson TF, Still WC. A rapid approximation to the solvent accessible surface areas of atoms. *Tetrahedron Comput Methodol*. 1988;1(2):103–16. doi:10.1016/0898-5529(88)90015-2.
  49. Hatherley D, Harlos K, Dunlop DC, Stuart DI, Barclay AN. The Structure of the macrophage signal regulatory protein α (SIRPα) inhibitory receptor reveals a binding face reminiscent of that used by T cell receptors. *J Biol Chem*. 2007;282(19):14567–75. doi:10.1074/jbc.M611511200.